A nonlinear POD-Galerkin reduced-order model for compressible flows taking into account rigid body motions

Antoine Placzek, Duc Minh Tran, Roger Ohayon

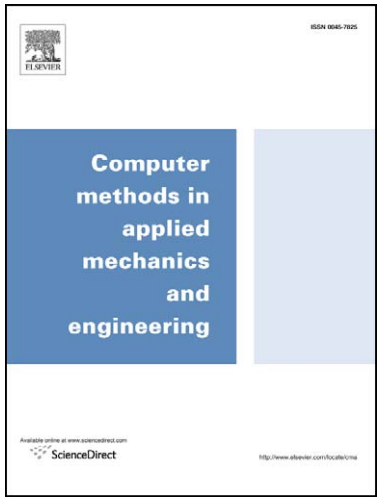

A nonlinear POD-Galerkin reduced-order model for compressible flows taking into account rigid body motions

A. Placzek, D.-M. Tran, R. Ohayon

PII: S0045-7825(11)00272-6
DOI: 10.1016/j.cma.2011.08.017
Reference: CMA 9540

To appear in: *Comput. Methods Appl. Mech. Engrg.*

Received Date: 15 December 2010
Revised Date: 17 August 2011
Accepted Date: 18 August 2011

Please cite this article as: A. Placzek, D.-M. Tran, R. Ohayon, A nonlinear POD-Galerkin reduced-order model for compressible flows taking into account rigid body motions, *Comput. Methods Appl. Mech. Engrg.* (2011), doi: 10.1016/j.cma.2011.08.017

A nonlinear POD-Galerkin reduced-order model for compressible flows taking into account rigid body motions

A. Placzek[a,*], D.-M. Tran[a], R. Ohayon[b]

[a] *ONERA, The French Aerospace Lab, F-92322 Châtillon, France*
[b] *Conservatoire National des Arts et Métiers, Structural Mechanics and Coupled Systems Laboratory, 2 rue Conté, 75003 Paris, France*

Abstract

The construction of a nonlinear reduced-order model for fluid-structure interaction problems is investigated in this paper for unsteady compressible flows excited by the rigid body motion of a structure. The reduction is achieved by means of a Galerkin projection of the Navier-Stokes equations on the first POD modes resulting from the Proper Orthogonal Decomposition. In the first part of the paper, the projection technique is carried out on a purely aerodynamic case in order (i) to validate an efficient iterative technique based on an updated QR decomposition to compute the POD modes, and (ii) to discuss the merits of different correction methods introduced to improve the long-term stability of the reduced-order model. The second and most original part of the paper deals with the construction of the reduced set of equations which arise from the projection of the compressible Navier-Stokes equations formulated in a suitable moving frame representing the rigid body motion. The expressions of the resulting non-autonomous terms appearing in the reduced-order model have also been optimized to reduce the computational costs.

Keywords: reduced-order model, proper orthogonal decomposition, Navier-Stokes, nonlinear, compressible flow, rigid body motion

1. Introduction

The modelization of unsteady aeroelastic phenomena like those involved in aircraft wings or turbomachinery is very time-consuming. Such simulations cannot be performed routinely for parametric studies which are needed to evaluate the performances and to control or optimize the system. Reduced-order models with a very small number of degrees of freedom are therefore developed since several decades in the hope of being able to reproduce almost the same dynamics as the full-order system. Specific reviews in the context of compressible aerodynamics have already been proposed [22, 45] but little work has been done in the case of fluid-structure interaction

*Corresponding author. Aeroelasticity and Structural Dynamics Department. Tel.: +33 1 46 73 45 80 – Fax: +33 1 46 73 41 43

Email addresses: antoine.placzek@onera.fr (A. Placzek), minh.tran_duc@onera.fr (D.-M. Tran), roger.ohayon@cnam.fr (R. Ohayon)

[4, 43, 63]. Another solution would be to consider the structural motion as a parameterized shape modification and to use sensitivity analysis to introduce the effects of the motion [1, 33, 34].

We focus here on the Proper Orthogonal Decomposition (POD) whose principle is to determine the optimal basis to represent the system response described by a set of snapshots [37]. On the assumption that the system variables can be decomposed on the POD basis at each time instant, the projection of the equations governing the mechanical system on each POD mode produces a small set of ordinary differential equations governing the coordinates of the variables in the basis.

Since the pioneer work of Lumley [47], the proper orthogonal decomposition has been extensively used as an efficient reduction method for a wide variety of fluid dynamics systems. Three main techniques have been developed according to the equations considered to model the flow. When the flow is linear or can be linearized, the *discrete projection* is the most straightforward technique since the projection is merely performed by means of a pre-multiplication by the transpose of the POD basis matrix. This type of reduced-order model has been widely used for linear stability analysis in the context of aircraft [44, 49] or turbomachinery applications [22, 23, 31, 67]. The nonlinearities can be preserved in the reduced-order model with what Lucia et al. [45] called the *projection on the residual*. At each time step, the nonlinear residual is computed in the physical space with the full-order model and is then projected on the POD basis to advance in time. This technique has been used successfully to reproduce large displacements effects [4], limit-cycles oscillations [8], or shock oscillations [46, 52]. The reduction is however not optimal since the aerodynamic field involving many degrees of freedom has to be reconstructed at each time instant to evaluate the residual. Recently Carlberg et al. [14] proposed an alternative formulation with three degrees of approximation to avoid the evaluation of the whole aerodynamic field. If the nonlinearity can be viewed as the action of multilinear operators like polynomials, the *Galerkin projection* technique yields an explicit nonlinear reduced-order model without requiring the computation of the residuals. Otherwise, the nonlinear terms are implicit and the technique has to cope with the same drawbacks as with the projection on the residual technique. The Galerkin projection approach already investigated by the author in [54] is therefore considered here. The main difficulty which is addressed in this paper lies in the formulation of the equations for compressible flows in the presence of a moving structure.

Indeed, the majority of the developments has focused on incompressible flows for which the Navier-Stokes equations are a set of quadratic partial differential equations. The Galerkin projection therefore leads to explicit nonlinear reduced-order models which have been used to reproduce turbulent structures [5, 11, 47], the vortex shedding process in the wake of obstacles [17, 40, 60] or behind a backward-facing step [18, 19] and the driven cavity flow problem [15, 40] for example. Recently, such reduced-order models have been applied to the control of flows [3, 10, 58, 59, 62, 66] or to fluid-structure interaction problems [43].

Three difficulties arise when dealing with POD-Galerkin reduced-order models for nonlinear compressible flows around a moving structure: the first one (i) is the choice of the variables to obtain polynomial equations, the second (ii) concerns the computation of the POD modes for large snapshots databases and the last one (iii) is related to the lack of stability.

The Navier-Stokes equations usually formulated with the conservative variables for compressible flows are not quadratic and the Galerkin projection yields an inadequate implicit formulation. For isentropic flows, Rowley et al. [57] managed to derive a quadratic reduced-order model

also employed in [29] to reproduce self-sustained oscillations of acoustic waves. In the general case, quadratic equations can yet be written with the judicious use of the modified primitive variables. This formulation has been introduced for nonlinear compressible flows around a *fixed* airfoil [12, 39, 64]. The main contribution of this paper is the extension of this formulation to solve point (i) in such a way that a *rigidly moving* structure can be taken into account in the Navier-Stokes equations while maintaining the quadratic form which is suitable for the projection.

Even with the snapshots method of Sirovich [61], the computation of the POD modes is time consuming as the snapshots become large. Solutions based on the Lanczos algorithm [24] or a parallel domain decomposition procedure [7] have been proposed, but the solution to point (ii) adopted here is based on a QR decomposition which is iteratively enriched [16, 48].

The lack of stability mentioned as point (iii) is due to the discretization scheme used to approximate the fluxes, to the truncation of the POD basis, to the non-respect of certain boundary conditions or to some simplifying assumptions [19, 38, 50, 56]. Numerous stabilization procedures have therefore been developed (see [29] for a comparison in the case of compressible flows). For autonomous systems, the proper evaluation of the initial conditions can be sufficient to reproduce accurately the limit-cycles [2]. The stability can also be enforced by modifying the dissipation operator [5, 15, 60, 64] or by replacing the usual L^2 inner product by another one which takes into account the spatial or temporal derivatives of the snapshots [35, 39, 41]. More sophisticated correction techniques based on the evaluation of the reduced-order model error have recently been developed [9, 40]. General calibration techniques have finally been introduced in [18, 27] to determine the optimal constant, linear and/or quadratic coefficients of the reduced-order model by minimizing an error functional. This technique has been formulated in [51, 66] as a linear least-squares problem.

In this paper, we consider as a preliminary work an oscillating airfoil in a nonlinear, compressible and possibly viscous flow. Such a level of modelization is indeed required to reproduce some complex aeroelastic phenomena [21] which motivate this study. Section 2 is devoted to the formulation of the POD-Galerkin reduced-order model for compressible flows governed by the Navier-Stokes equations described in a moving frame of reference with the set of modified primitive variables. The algorithm to compute the POD modes is also briefly described. In section 3, the correction techniques used to improve the accuracy of the reduced system response are presented. A first reduced-order model of the Navier-Stokes equations is constructed in section 4 for a fixed airfoil to validate the iterative QR decomposition algorithm adopted to compute the POD modes. Different calibration methods are also evaluated for short- and long-term time integration. Finally, a reduced-order model of the Euler equations is built in section 5 to reproduce the motion of a shock generated by the oscillation of a moving airfoil.

2. Construction of the POD-Galerkin reduced-order model for compressible flows

2.1. Computation of the POD modes

Let $Q = \{\boldsymbol{q}^{(m)} \in H; m = 1,..,M\}$ be a finite set of snapshots. Each snapshot is the solution of the full-order mechanical system at the time instant $t_m \in I_s = [t_0; t_0 + T_s]$ and is defined on the spatial domain $\Omega \subset \mathbb{R}^d$ with $d = 1, 2$ or 3 such that $\boldsymbol{q}^{(m)} = [q_1(t_m), \ldots, q_{n_v}(t_m)]^\mathsf{T}$ is a vector of

n_v squared integrable functions of space describing the aerodynamic field. The associated Hilbert space $H = (L^2(\Omega))^{n_v}$ is endowed for all $\boldsymbol{q}$ and $\boldsymbol{r}$ in H with the inner product

$$\langle \boldsymbol{q}, \boldsymbol{r} \rangle = \int_\Omega \sum_{k=1}^{n_v} q_k \, r_k \, \mathrm{d}\Omega, \tag{1}$$

and the induced norm is $\|\boldsymbol{q}\|^2 = \langle \boldsymbol{q}, \boldsymbol{q} \rangle$. The previous inner product is well-defined as long as the snapshots are dimensionless since they contain different physical quantities.

The aim of the proper orthogonal decomposition is to find a subspace $S \subset H$ of low dimension q which provides the best approximation of any member of Q. Usually the snapshots are *centered* and the problem is to find the best basis to approximate the fluctuations of the snapshots $\widetilde{\boldsymbol{q}}^{(m)} = \boldsymbol{q}^{(m)} - \overline{\boldsymbol{q}}$ around a mean state defined by the discrete weighted temporal average $\overline{\boldsymbol{q}} = E[\boldsymbol{q}^{(m)}] = \sum_{m=1}^{M} \alpha_m \boldsymbol{q}^{(m)}$ with $\alpha_m > 0$ and $\sum_{m=1}^{M} \alpha_m = 1$. The subspace is defined by the basis $\Phi = \{\varphi^{(j)} \in H; j = 1, .., q\}$ so that $S = \mathrm{span}\{\varphi^{(1)}, ..., \varphi^{(q)}\}$. Each snapshot $\boldsymbol{q}^{(m)}$ can therefore be approximated on the subspace S by the following affine decomposition on the POD modes $\varphi^{(j)}$:

$$\boldsymbol{q}^{(m)} \approx \boldsymbol{q}^{(m)}_{\mathrm{POD}} = \overline{\boldsymbol{q}} + \sum_{j=1}^{q} a_j^{(m)} \, \varphi^{(j)} \quad \forall m \in [\![1; M]\!]. \tag{2}$$

The optimality statement of the POD modes $\varphi^{(j)}$ and the additional constraints of orthonormality lead to the definition [42]

$$\begin{cases} \min\limits_{\varphi^{(j)} \in H} E\left[\left\| \widetilde{\boldsymbol{q}}^{(m)} - \sum\limits_{j=1}^{q} \left\langle \widetilde{\boldsymbol{q}}^{(m)}, \varphi^{(j)} \right\rangle \varphi^{(j)} \right\|^2 \right] \\ \text{subject to } \left\langle \varphi^{(i)}, \varphi^{(j)} \right\rangle = \delta_{ij} \end{cases} \tag{3}$$

which is equivalent to the maximization of $\sum_{j=1}^{q} \langle E[\langle \widetilde{\boldsymbol{q}}^{(m)}, \varphi^{(j)} \rangle \widetilde{\boldsymbol{q}}^{(m)}], \varphi^{(j)} \rangle$ [54]. Introducing the linear operator R such that for all $\boldsymbol{y} \in H$, $R\boldsymbol{y} = E[\langle \widetilde{\boldsymbol{q}}^{(m)}, \boldsymbol{y} \rangle \widetilde{\boldsymbol{q}}^{(m)}]$, the optimization problem (3) finally amounts to the resolution of the eigenvalue problem $R\varphi^{(j)} = \lambda_j \varphi^{(j)}$ for each POD mode $\varphi^{(j)}$ [37, 54]. This approach is called the *direct method* since the POD modes are directly computed as the solutions of the eigenproblem. The Hilbert-Schmidt operator R has $r \leq M$ non-null eigenvalues and eigenvectors. The eigenvalues λ_j represent the "energy" captured by each POD mode and provide an estimation of the truncation error $\varepsilon_q = \sum_{j=q+1}^{r} \lambda_j$ [42].

After discretization, the set of snapshots is approximated by the real matrix $\widetilde{\mathbf{Q}} \in \mathscr{M}(N_v, M)$ whose general term is $q_i^{(m)} - \overline{q}_i$ and the linear operator R can be represented by the matrix $\mathbf{R} \in \mathscr{M}(N_v, N_v)$. For that purpose, the spatial domain is split in N discretization elements Ω_e such that $\Omega = \bigcup_{e=1}^{N} \Omega_e$ and the integral in Eq. (1) is approximated by the trapezoidal rule such that $\langle \boldsymbol{q}, \boldsymbol{r} \rangle \approx \sum_{e=1}^{N} \sum_{k=1}^{n_v} q_{k,e} \, r_{k,e} \, \delta\Omega_e$, where $\delta\Omega_e$ is the Lebesgue measure of the discretization element Ω_e and $q_{k,e}$ (resp. $r_{k,e}$) is the spatial average value of q_k (resp. r_k) evaluated at the center of the element. Denoting $N_v = n_v N$, the i-th component of the vector $R\varphi^{(j)}$ writes $(R\varphi^{(j)})_i \approx \sum_{n=1}^{N_v} (\sum_{m=1}^{M} \alpha_m \widetilde{q}_n^{(m)} \widetilde{q}_i^{(m)} \Delta_n) \, \varphi_n^{(j)}$ and the general term of the matrix $\mathbf{R}$ is therefore the

spatial weighted covariance $\sum_{m=1}^{M} \alpha_m \widetilde{q}_n^{(m)} \widetilde{q}_i^{(m)} \Delta_n$. We introduce finally the diagonal matrix $\widetilde{\alpha}$ containing the square roots of the weights α_m, the block diagonal matrix $\widetilde{\Delta}$ containing the square roots of the Lebesgue measures $\delta\Omega_n$ and the weighted snapshot matrix $\widehat{\mathbf{Q}} = \widetilde{\Delta}\widetilde{\mathbf{Q}}\widetilde{\alpha}$ such that the linear operator of the direct method is defined by the matrix product $\mathbf{R} = \widehat{\mathbf{Q}}\widehat{\mathbf{Q}}^{\mathsf{T}} \in \mathscr{M}(N_v, N_v)$.

The computation of the eigenvectors of $\mathbf{R}$ becomes very costly when the number N_v of degrees of freedom is large. The *snapshots method* [61] thus reduces considerably the size of the eigenproblem. It is based on the linear decomposition of the POD modes on the snapshots:

$$\varphi^{(j)} = \sum_{m=1}^{M} c_m^{(j)} \widetilde{\boldsymbol{q}}^{(m)}. \tag{4}$$

The eigenvalue problem $R\varphi^{(j)} = \lambda_j \varphi^{(j)}$ of the direct method is replaced by the following $M \times M$ problem involving the temporal covariance matrix $\mathbf{R}^\star$ [54, 61]:

$$\mathbf{R}^\star \mathbf{d}^{(j)} = \lambda_j \mathbf{d}^{(j)}, \tag{5}$$

with $R^\star_{ij} = \sqrt{\alpha_i \alpha_j}\langle \widetilde{\boldsymbol{q}}^{(i)}, \widetilde{\boldsymbol{q}}^{(j)} \rangle$. The POD modes are now defined by Eq. (4) and the relation $\mathbf{c}^{(j)} = \widetilde{\alpha}\mathbf{d}^{(j)}$. The temporal covariance matrix is in practice computed as the matrix product $\mathbf{R}^\star = \widehat{\mathbf{Q}}^{\mathsf{T}}\widehat{\mathbf{Q}} \in \mathscr{M}(M, M)$. If $M \ll N_v$ the evaluation of the POD modes is much less costly.

However the snapshots method has still two main drawbacks. First, the evaluation of the covariance matrix $\mathbf{R}^\star$ can lead to severe round-off errors [30]. Second, the full snapshots matrix may exceed the memory size available and the construction of the covariance matrix requires $M \times (M+1)/2$ files reading if the snapshots are stored in separate files. The POD modes are finally obtained after M additional readings of the snapshots since they are defined by Eq. (5).

An alternative solution is to compute the singular value decomposition (SVD) of the weighted snapshots matrix $\widehat{\mathbf{Q}} = \mathbf{Q}_{1,r}\Sigma_r\mathbf{Q}_{2,r}^{\mathsf{T}}$, where $\mathbf{Q}_{1,r} \in \mathscr{M}(N_v, r)$ contains the left singular vectors, $\mathbf{Q}_{2,r} \in \mathscr{M}(M, r)$ contains the right singular vectors and $\Sigma_r \in \mathscr{M}(r, r)$ is the diagonal matrix containing the r non-null singular values σ_j [30]. The left singular vectors are the POD modes [65] since $\mathbf{R} = \mathbf{Q}_{1,r}\Sigma_r^2\mathbf{Q}_{1,r}^{\mathsf{T}}$ and the POD eigenvalues are $\lambda_j = \sigma_j^2$. Similarly, the right singular vectors are the eigenvectors of the operator $\mathbf{R}^\star$ since $\mathbf{R}^\star = \mathbf{Q}_{2,r}\Sigma_r^2\mathbf{Q}_{2,r}^{\mathsf{T}}$. The definition of the POD modes as the left eigenvectors of $\widehat{\mathbf{Q}}$ does not introduce any round-off errors since the evaluation of the covariance matrix is not needed. This solution is however only possible if the full snapshots matrix can be stored in memory so that the SVD is performed for all snapshots at once.

The solution adopted here is to consider the first q snapshots as an initial approximation of the left singular subspace and to improve it iteratively [16]. In this way, only the first q POD modes are computed whereas the whole basis is computed with the snapshots method and is then truncated.

The initial sub-matrix $\widehat{\mathbf{Q}}_q \in \mathscr{M}(N_v, q)$ containing the first $q \leq M$ snapshots is factored by a QR decomposition such that $\widehat{\mathbf{Q}}_q = \mathbf{Q}_q\mathbf{R}_q$. Then for $i = q+1$ to M the i-th column $\widehat{\boldsymbol{q}}^{(i)}$ of the snapshots matrix $\widehat{\mathbf{Q}}$ is appended to $\widehat{\mathbf{Q}}_{i-1}$. At each iteration of the algorithm, the extended matrix $\widehat{\mathbf{Q}}_{\text{up}} = [\widehat{\mathbf{Q}}_{i-1}, \widehat{\boldsymbol{q}}^{(i)}]$ is therefore updated with the relation

$$\widehat{\mathbf{Q}}_{\text{up}} = \begin{bmatrix}\mathbf{Q}_{i-1}\mathbf{R}_{i-1} & \widehat{\boldsymbol{q}}^{(i)}\end{bmatrix} = \begin{bmatrix}\mathbf{Q}_{i-1} & \theta_i\end{bmatrix} \begin{bmatrix}\mathbf{R}_{i-1} & \mathbf{r}_i \\ \mathbf{0} & \rho_i\end{bmatrix} = \widetilde{\mathbf{Q}}_i\widetilde{\mathbf{R}}_i \tag{6}$$

by means of a Gram-Schmidt orthogonalization. The last singular vector $\mathbf{u}_{q+1}$ of $\widetilde{\mathbf{R}}_i$ is computed as well as the last singular value σ_{q+1} and an orthogonal transformation $\mathbf{G}_u$ is computed such that $\mathbf{G}_u^{\mathsf{T}}\mathbf{u}_{q+1} = \mathbf{e}_{q+1}$. Finally the orthogonal transformation $\mathbf{G}_v$ is determined to put back $\mathbf{G}_u^{\mathsf{T}}\widetilde{\mathbf{R}}_i$ in the upper triangular form $\mathbf{R}_{\text{up}} = \mathbf{G}_u^{\mathsf{T}}\widetilde{\mathbf{R}}_i\mathbf{G}_v$ and the matrix $\widetilde{\mathbf{Q}}_i$ is updated in $\mathbf{Q}_{\text{up}} = \widetilde{\mathbf{Q}}_i\mathbf{G}_u$. The extended matrix is thus updated in $\widehat{\mathbf{Q}}_{\text{up}} = \mathbf{Q}_{\text{up}}\mathbf{R}_{\text{up}}\mathbf{G}_v^{\mathsf{T}}$ and $\widehat{\mathbf{Q}}_i$ is defined as the first q columns of $\widehat{\mathbf{Q}}_{\text{up}}$. The corresponding QR approximation of $\widehat{\mathbf{Q}}_i$ is thus given by $\mathbf{Q}_i$ and $\mathbf{R}_i$ where the last column (and row for $\mathbf{R}_i$) has been eliminated. At the end of the iterations, the matrix $\widehat{\mathbf{Q}}_M$ contains the information of all snapshots and can be used to evaluate the POD modes. The algorithm used in this paper is detailed in Appendix A. Improvements of the previous algorithm have been proposed to decrease further the computational costs [48].

The cost of this solution to compute the POD modes is low since the update of the subspace involves only small matrices which can be stored in memory and the algorithm requires only one reading of each snapshot. The computation does not involve the covariance matrix and round-off errors are thus reduced. This approach is also particularly interesting if the snapshots database is completed later: additional snapshots can be taken into account without building again a covariance matrix like in the snapshots method. This could be useful if the POD modes are constructed from different simulations or if the simulation is pursued further in time.

2.2. Construction of the POD-Galerkin reduced-order model

The Navier-Stokes equations for compressible flows are usually written with the conservative variables. They are however not appropriate to build a reduced-order model in the framework of a Galerkin projection because of the apparition of rational fractions which produce an implicit formulation of the reduced-order model. In the case of a fixed structure (and thus an invariant domain), polynomial quadratic equations are yet obtained if the fluid equations are formulated with the modified primitive variables $\boldsymbol{q} = [\vartheta, \boldsymbol{u}, p]^{\mathsf{T}}$, where $\vartheta = 1/\rho$ is the covolume, $\boldsymbol{u}$ is the vector of the velocity components and p is the pressure [39, 64].

The main purpose of this paper is to extend this formulation in such a way that the motion of a structure can be taken into account while maintaining a polynomial form of the equations which is adequate for the Galerkin projection. We therefore consider the Arbitrary Lagrangian-Eulerian (ALE) formulation [20] of the Navier-Stokes equations which modifies the convective terms by the introduction of the mesh velocity $\boldsymbol{s}$ split into the velocity $\boldsymbol{s}_{\text{mfr}}$ of the moving frame of reference and the deformation velocity $\boldsymbol{s}_d$.

These velocities stem from the definition of the absolute position $\boldsymbol{x}$ of a point $M \in \Omega$ which writes $\boldsymbol{x} = \boldsymbol{x}_0 + \widetilde{\boldsymbol{x}}$ with $\boldsymbol{x}_0$ the position of the origin M_0 of the moving frame and $\widetilde{\boldsymbol{x}}$ the relative position of the point M in the moving frame. The relative position is also defined by $\widetilde{\boldsymbol{x}} = \mathbf{P}\widetilde{\boldsymbol{x}}_{\text{mfr}}$ where $\mathbf{P}$ is the change of basis matrix between the absolute and moving frames and $\widetilde{\boldsymbol{x}}_{\text{mfr}}$ is the relative position whose components are expressed in the moving frame. Using the previous relations, the velocity $\boldsymbol{s}_{\text{mfr}}$ of the moving frame and the deformation velocity $\boldsymbol{s}_d$ are defined by

$$\boldsymbol{s}_{\text{mfr}} = \boldsymbol{s}_0 + \boldsymbol{\omega} \wedge \widetilde{\boldsymbol{x}}_{\text{mfr}} \quad \text{and} \quad \boldsymbol{s}_d = \frac{\mathrm{d}\widetilde{\boldsymbol{x}}_{\text{mfr}}}{\mathrm{d}t}, \tag{7}$$

where $\boldsymbol{s}_0 = \mathbf{P}^{\mathsf{T}}(\mathrm{d}\boldsymbol{x}_0/\mathrm{d}t)$ is the velocity of the origin of the moving frame and $\boldsymbol{\omega}$ is a rotation vector associated to the skew-symmetric matrix $\mathbf{P}^{\mathsf{T}}(\mathrm{d}\mathbf{P}/\mathrm{d}t)$.

The dimensionless Navier-Stokes equations derived from the classical conservation equations for the mass, the momentum and the energy [6] are finally written with the modified primitive variables in the moving frame associated to the rigid body motion of the structure. The components of the velocity vector $\boldsymbol{u}$, as well as the spatial differentiation operators, are expressed in the moving frame and the conservation equations become [53]

$$\begin{cases} \dfrac{\partial \vartheta}{\partial t} + (\boldsymbol{u}-\boldsymbol{s})\cdot\nabla\vartheta = \vartheta \operatorname{div}\boldsymbol{u} \\ \dfrac{\partial \boldsymbol{u}}{\partial t} + (\boldsymbol{u}-\boldsymbol{s})\cdot\nabla\boldsymbol{u} = -\vartheta\nabla p + \dfrac{\vartheta}{\mathrm{Re}}\operatorname{div}\tau_{\mu_r}(\boldsymbol{u}) - \boldsymbol{\omega}\wedge\boldsymbol{u} \\ \dfrac{\partial p}{\partial t} + (\boldsymbol{u}-\boldsymbol{s})\cdot\nabla p \ = -\gamma p \operatorname{div}\boldsymbol{u} + \dfrac{\gamma-1}{\mathrm{Re}}\nabla\boldsymbol{u} : \tau_{\mu_r}(\boldsymbol{u}) \\ \qquad\qquad + \dfrac{\gamma}{\mathrm{Re}\,\mathrm{Pr}}\Delta(\vartheta\, p), \end{cases} \tag{8}$$

where $\gamma = c_p/c_v$ is the heat capacity ratio, c_p and c_v are the specific heat capacities and Re and Pr are respectively the dimensionless Reynolds and Prandtl numbers defined for a reference viscosity μ_r and the thermal conductivity k_θ. For a Newtonian fluid, the viscous stress tensor is defined by $\tau(\boldsymbol{u}) = 2\mu\boldsymbol{D} - 2/3\,\mu(\operatorname{div}\boldsymbol{u})\boldsymbol{I}_d$ where $\boldsymbol{D} = 1/2(\nabla\boldsymbol{u} + \nabla^{\mathsf{T}}\boldsymbol{u})$ is the rate of deformation tensor. The dimensionless viscous stress tensor $\tau_{\mu_r}(\boldsymbol{u}) = (\nabla\boldsymbol{u} + \nabla^{\mathsf{T}}\boldsymbol{u}) - 2/3\,(\operatorname{div}\boldsymbol{u})\,\boldsymbol{I}_d$ stem from the division of the viscous stress tensor τ by μ_r which is here assumed to be constant and equal to the fluid viscosity μ (although it depends on the temperature via the Sutherland law and can be modified by the turbulence). Finally, the thermal conductivity k_θ and the specific heat capacity c_v are assumed to be constant since we consider a perfect gas.

A second formulation similar to Eqs. (8) for the Navier-Stokes equations formulated in the reference frame can be obtained by substituting the absolute velocity $\boldsymbol{u}$ with the relative velocity $\boldsymbol{v} = \boldsymbol{u} - \boldsymbol{s}_{\text{mfr}}$ and leads to the apparition of the usual Coriolis and centrifugal forces [53].

When the structure is moving or deforming, the spatial domain is no longer invariant and the inner product Eq. (1) is ill-defined since two snapshots taken at different time instants are not defined on the same spatial domain [43]. However if the structure is restricted to rigid body motions, the fluid equations (8) formulated in the moving frame associated to the motion amounts to consider an invariant spatial domain and the inner product is well-defined. If the structure is deforming, the formulation has to be adapted by an approach similar to [43] which should be extended for compressible flows. In this paper we only consider rigid body motions such that the mesh velocity $\boldsymbol{s} = \boldsymbol{s}_{\text{mfr}} + \boldsymbol{s}_d$ is just defined by the velocity of the moving frame $\boldsymbol{s}_{\text{mfr}} = \boldsymbol{s}_0 + \boldsymbol{\omega}\wedge\widetilde{\boldsymbol{x}}_{\text{mfr}}$ since $\boldsymbol{s}_d = 0$. The Navier-Stokes equations (8) therefore write under the generic quadratic form

$$\dot{\boldsymbol{q}} = \mathbf{Q}^C(\boldsymbol{q},\boldsymbol{q}) + \frac{1}{\mathrm{Re}}\mathbf{Q}^D(\boldsymbol{q},\boldsymbol{q}) + \mathbf{T}(\boldsymbol{q},\boldsymbol{s}_0,\boldsymbol{\omega}), \tag{9}$$

where the convective, diffusive and source terms are defined as multilinear operators by :

$$\mathbf{Q}^C(\boldsymbol{q},\boldsymbol{q}) = \begin{bmatrix} -\boldsymbol{u}\cdot\nabla\vartheta + \vartheta\operatorname{div}\boldsymbol{u} \\ -\boldsymbol{u}\cdot\nabla\boldsymbol{u} - \vartheta\nabla p \\ -\boldsymbol{u}\cdot\nabla p - \gamma p\operatorname{div}\boldsymbol{u} \end{bmatrix}, \tag{10a}$$

$$\mathbf{Q}^D(\boldsymbol{q},\boldsymbol{q}) = \begin{bmatrix} 0 \\ \vartheta \,\mathrm{div}\, \tau_{\mu_r}(\boldsymbol{u}) \\ (\gamma-1)\nabla\boldsymbol{u} : \tau_{\mu_r}(\boldsymbol{u}) + \dfrac{\gamma}{\mathrm{Pr}}\Delta(\vartheta\, p) \end{bmatrix}, \tag{10b}$$

$$\mathbf{T}(\boldsymbol{q},\boldsymbol{s}_0,\boldsymbol{\omega}) = \begin{bmatrix} \boldsymbol{s}_{\mathrm{mfr}}\cdot\nabla\vartheta \\ \boldsymbol{s}_{\mathrm{mfr}}\cdot\nabla\boldsymbol{u} - \boldsymbol{\omega}\wedge\boldsymbol{u} \\ \boldsymbol{s}_{\mathrm{mfr}}\cdot\nabla p \end{bmatrix}. \tag{10c}$$

The flow variables are approximated at each time instant t by an affine decomposition similar to (2). The modal amplitudes $a_j^{(m)}$ which were known at the time instants t_m associated to the snapshots are now the unknown coefficients $a_j(t)$ for which the reduced-order model is built. The decomposition $\boldsymbol{q}(t) = \overline{\boldsymbol{q}} + \sum_{j=1}^{q} a_j(t)\,\boldsymbol{\varphi}^{(j)}$ is introduced into the system of equations (9). Using the multilinearity of the spatial operators $\mathbf{Q}^C$, $\mathbf{Q}^D$ and $\mathbf{T}$, the Galerkin projection on each POD mode $\boldsymbol{\varphi}^{(i)}$ produces the set of q nonlinear, non-autonomous, quadratic ordinary differential equations :

$$\begin{aligned} \dot{a}_i(t) = \mathscr{K}_i + \sum_{j=1}^{q} \mathscr{L}_{ij}\, a_j(t) + \sum_{j,k=1}^{q} \mathscr{Q}_{jik}\, a_j(t)\, a_k(t) \\ + \mathscr{K}_i^{\mathrm{mfr}}(t) + \sum_{j=1}^{q} \mathscr{L}_{ij}^{\mathrm{mfr}}(t)\, a_j(t). \end{aligned} \tag{11}$$

The constant, linear and quadratic coefficients defining the autonomous part of the polynomial equations (11) can be decomposed in $\mathscr{C} = \mathscr{C}^C + 1/\mathrm{Re}\,\mathscr{C}^D$ where $\mathscr{C}$ denotes either $\mathscr{K}_i$, $\mathscr{L}_{ij}$ or $\mathscr{Q}_{ijk}$. The expressions of the coefficients are detailed below:

$$\begin{cases} \mathscr{K}_i^C = \left\langle \mathbf{Q}^C(\overline{\mathbf{q}},\overline{\mathbf{q}}), \boldsymbol{\varphi}^{(i)} \right\rangle \\ \mathscr{K}_i^D = \left\langle \mathbf{Q}^D(\overline{\mathbf{q}},\overline{\mathbf{q}}), \boldsymbol{\varphi}^{(i)} \right\rangle \end{cases} \tag{12a}$$

$$\begin{cases} \mathscr{L}_{ij}^C = \left\langle \mathbf{Q}^C\left(\overline{\mathbf{q}},\boldsymbol{\varphi}^{(j)}\right) + \mathbf{Q}^C\left(\boldsymbol{\varphi}^{(j)},\overline{\mathbf{q}}\right), \boldsymbol{\varphi}^{(i)} \right\rangle \\ \mathscr{L}_{ij}^D = \left\langle \mathbf{Q}^D\left(\overline{\mathbf{q}},\boldsymbol{\varphi}^{(j)}\right) + \mathbf{Q}^D\left(\boldsymbol{\varphi}^{(j)},\overline{\mathbf{q}}\right), \boldsymbol{\varphi}^{(i)} \right\rangle \end{cases} \tag{12b}$$

$$\begin{cases} \mathscr{Q}_{ijk}^C = \left\langle \mathbf{Q}^C\left(\boldsymbol{\varphi}^{(j)},\boldsymbol{\varphi}^{(k)}\right), \boldsymbol{\varphi}^{(i)} \right\rangle \\ \mathscr{Q}_{ijk}^D = \left\langle \mathbf{Q}^D\left(\boldsymbol{\varphi}^{(j)},\boldsymbol{\varphi}^{(k)}\right), \boldsymbol{\varphi}^{(i)} \right\rangle \end{cases} \tag{12c}$$

$$\begin{cases} \mathscr{K}_i^{\mathrm{mfr}}(t) = \left\langle \mathbf{T}(\overline{\mathbf{q}},\boldsymbol{s}_0,\boldsymbol{\omega}), \boldsymbol{\varphi}^{(i)} \right\rangle \\ \mathscr{L}_{ij}^{\mathrm{mfr}}(t) = \left\langle \mathbf{T}\left(\boldsymbol{\varphi}^{(j)},\boldsymbol{s}_0,\boldsymbol{\omega}\right), \boldsymbol{\varphi}^{(i)} \right\rangle. \end{cases} \tag{12d}$$

If the projection basis contains q POD modes, the total number of autonomous coefficients to compute is $N_c^{\mathrm{a}} = q(q+1)(q+2)/2$. Because of the motion of the domain, there are $N_c^{\mathrm{na}} = q + q^2$ additional non-autonomous constant and linear coefficients $\mathscr{K}_i^{\mathrm{mfr}}(t)$ and $\mathscr{L}_{ij}^{\mathrm{mfr}}(t)$ to compute.

The expressions of the quadratic coefficients are detailed in the following when the quadratic operators $\mathbf{Q}^C$ and $\mathbf{Q}^D$ are applied to $(\varphi^{(j)},\varphi^{(k)})$. The expressions of the linear and constant coefficients can be deduced by substituting the couple $(\varphi^{(j)},\varphi^{(k)})$ by $(\varphi^{(j)},\overline{\boldsymbol{q}})$ and $(\overline{\boldsymbol{q}},\overline{\boldsymbol{q}})$ respectively. The POD modes are split into $\varphi^{(j)}=[\varphi_\vartheta^{(j)},\varphi_{\boldsymbol{u}}^{(i)},\varphi_p^{(j)}]^\mathsf{T}$ and the development of Eqs. (12c) leads to

$$\begin{aligned}\mathscr{Q}^C_{ijk}=&-\int_\Omega\left(\varphi_{\boldsymbol{u}}^{(j)}\cdot\nabla\varphi_\vartheta^{(k)}-\varphi_\vartheta^{(k)}\operatorname{div}\varphi_{\boldsymbol{u}}^{(j)}\right)\varphi_\vartheta^{(i)}\,\mathrm{d}\Omega\\&-\int_\Omega\left(\varphi_{\boldsymbol{u}}^{(j)}\cdot\nabla\varphi_{\boldsymbol{u}}^{(k)}+\varphi_\vartheta^{(j)}\nabla\varphi_p^{(k)}\right)\cdot\varphi_{\boldsymbol{u}}^{(i)}\,\mathrm{d}\Omega\\&-\int_\Omega\left(\varphi_{\boldsymbol{u}}^{(j)}\cdot\nabla\varphi_p^{(k)}+\gamma\varphi_p^{(j)}\operatorname{div}\varphi_{\boldsymbol{u}}^{(k)}\right)\varphi_p^{(i)}\,\mathrm{d}\Omega\end{aligned}\tag{13}$$

and

$$\begin{aligned}\mathscr{Q}^D_{ijk}=&\int_\Omega\varphi_\vartheta^{(j)}\operatorname{div}\tau_{\mu_r}\left(\varphi_{\boldsymbol{u}}^{(k)}\right)\cdot\varphi_{\boldsymbol{u}}^{(i)}\,\mathrm{d}\Omega\\&+\int_\Omega\left[(\gamma-1)\nabla\varphi_{\boldsymbol{u}}^{(j)}:\tau_{\mu_r}\left(\varphi_{\boldsymbol{u}}^{(k)}\right)\right]\varphi_p^{(i)}\,\mathrm{d}\Omega\\&+\int_\Omega\left[\frac{\gamma}{\mathrm{Pr}}\Delta\left(\varphi_\vartheta^{(j)}\varphi_p^{(k)}\right)\right]\varphi_p^{(i)}\,\mathrm{d}\Omega.\end{aligned}\tag{14}$$

The Green-Ostrogradski theorem is then employed as a generalized integration by parts tool in order to avoid the computation of the second order spatial derivatives involved in the diffusive coefficients defined according to Eq. (14) by $\mathscr{Q}^D_{ijk}=\widetilde{\mathscr{Q}}^D_{\boldsymbol{u}}+(\gamma-1)\,\widetilde{\mathscr{Q}}^D_{p,1}+\gamma/\mathrm{Pr}\,\widetilde{\mathscr{Q}}^D_{p,2}$. This theorem states for any vector $\boldsymbol{v}$ defined in Ω bounded by $\partial\Omega$ with the normal $\boldsymbol{n}$ that $\int_\Omega\operatorname{div}\boldsymbol{v}\,\mathrm{d}\Omega=\oint_{\partial\Omega}\boldsymbol{v}\cdot\boldsymbol{n}\,\mathrm{d}\partial\Omega$. Consequently, for a scalar $s=\varphi_\vartheta^{(j)}$, a vector $\boldsymbol{v}=\varphi_{\boldsymbol{u}}^{(i)}$ and a matrix $\boldsymbol{M}=\tau_{\mu_r}(\varphi_{\boldsymbol{u}}^{(k)})$, the integrand of the term $\widetilde{\mathscr{Q}}^D_{\boldsymbol{u}}$ becomes $s\operatorname{div}\boldsymbol{M}\cdot\boldsymbol{v}=\operatorname{div}(s\,\boldsymbol{v}^\mathsf{T}\boldsymbol{M})-s\nabla\boldsymbol{v}:\boldsymbol{M}-(\boldsymbol{v}\otimes\nabla s):\boldsymbol{M}$ and the application of the Green-Ostrogradski theorem to the vector $s\,\boldsymbol{v}^\mathsf{T}\boldsymbol{M}$ leads to

$$\begin{aligned}\widetilde{\mathscr{Q}}^D_{\boldsymbol{u}}=&\oint_{\partial\Omega}\left[\varphi_\vartheta^{(j)}\left(\varphi_{\boldsymbol{u}}^{(i)}\right)^\mathsf{T}\tau_{\mu_r}\left(\varphi_{\boldsymbol{u}}^{(k)}\right)\right]\boldsymbol{n}\,\mathrm{d}\partial\Omega\\&-\int_\Omega\varphi_\vartheta^{(j)}\nabla\varphi_{\boldsymbol{u}}^{(i)}:\tau_{\mu_r}\left(\varphi_{\boldsymbol{u}}^{(k)}\right)\mathrm{d}\Omega\\&-\int_\Omega\left(\varphi_{\boldsymbol{u}}^{(i)}\otimes\nabla\varphi_\vartheta^{(j)}\right):\tau_{\mu_r}\left(\varphi_{\boldsymbol{u}}^{(k)}\right)\mathrm{d}\Omega.\end{aligned}\tag{15}$$

The second term $\widetilde{\mathscr{Q}}^D_{p,1}$ in (14) is not modified since it involves only first order derivatives. The third term $\widetilde{\mathscr{Q}}^D_{p,2}$ also writes $q\,\Delta(rs)=q\operatorname{div}(\nabla(rs))=\operatorname{div}[q\nabla(rs)]-r\nabla s\cdot\nabla q-s\nabla r\cdot\nabla q$ with $q=\varphi_p^{(i)}$, $r=\varphi_\vartheta^{(j)}$ and $s=\varphi_p^{(k)}$. Using the Green-Ostrogradski theorem for the vector $q\nabla(rs)$, the term $\widetilde{\mathscr{Q}}^D_{p,2}$ is then transformed into

$$\begin{aligned}\widetilde{\mathscr{Q}}^D_{p,2}=&\oint_{\partial\Omega}\varphi_p^{(i)}\nabla\left(\varphi_\vartheta^{(j)}\varphi_p^{(k)}\right)\cdot\boldsymbol{n}\,\mathrm{d}\partial\Omega\\&-\int_\Omega\varphi_\vartheta^{(j)}\nabla\varphi_p^{(k)}\cdot\nabla\varphi_p^{(i)}\,\mathrm{d}\Omega\\&-\int_\Omega\varphi_p^{(k)}\nabla\varphi_\vartheta^{(j)}\cdot\nabla\varphi_p^{(i)}\,\mathrm{d}\Omega.\end{aligned}\tag{16}$$

The different contributions produced by the integration by parts are finally combined so that the diffusive term $\mathscr{Q}^D_{ijk} = \mathscr{Q}^D_{\text{Vol}} + \mathscr{Q}^D_{\text{Surf}}$ is decomposed into volume and surface contributions which involve only first order spatial derivatives. The expressions are given by:

$$\begin{aligned}
\mathscr{Q}^D_{\text{Vol}} &= -\int_\Omega \varphi^{(j)}_\vartheta \nabla\varphi^{(i)}_{\boldsymbol{u}} : \tau_{\mu_r}\left(\varphi^{(k)}_{\boldsymbol{u}}\right)\mathrm{d}\Omega \\
&- \int_\Omega \left(\varphi^{(i)}_{\boldsymbol{u}} \otimes \nabla\varphi^{(j)}_\vartheta\right) : \tau_{\mu_r}\left(\varphi^{(k)}_{\boldsymbol{u}}\right)\mathrm{d}\Omega \\
&+ (\gamma-1)\int_\Omega \nabla\varphi^{(j)}_{\boldsymbol{u}} : \tau_{\mu_r}\left(\varphi^{(k)}_{\boldsymbol{u}}\right)\varphi^{(i)}_p\,\mathrm{d}\Omega \\
&- \frac{\gamma}{\mathrm{Pr}}\int_\Omega \varphi^{(j)}_\vartheta \nabla\varphi^{(k)}_p \cdot \nabla\varphi^{(i)}_p\,\mathrm{d}\Omega \\
&- \frac{\gamma}{\mathrm{Pr}}\int_\Omega \varphi^{(k)}_p \nabla\varphi^{(j)}_\vartheta \cdot \nabla\varphi^{(i)}_p\,\mathrm{d}\Omega,
\end{aligned} \tag{17a}$$

$$\begin{aligned}
\mathscr{Q}^D_{\text{Surf}} &= \oint_{\partial\Omega}\left[\varphi^{(j)}_\vartheta \left(\varphi^{(i)}_{\boldsymbol{u}}\right)^{\mathsf{T}} \tau_{\mu_r}\left(\varphi^{(k)}_{\boldsymbol{u}}\right)\right]\boldsymbol{n}\,\mathrm{d}\partial\Omega \\
&+ \frac{\gamma}{\mathrm{Pr}}\oint_{\partial\Omega}\varphi^{(i)}_p \nabla\left(\varphi^{(j)}_\vartheta\,\varphi^{(k)}_p\right)\cdot\boldsymbol{n}\,\mathrm{d}\partial\Omega.
\end{aligned} \tag{17b}$$

The autonomous coefficients of the reduced-order model are thus completely defined by the expressions (12), (13) and (17). The expressions of the non-autonomous coefficients given by Eqs. (12d) are time-dependent and their evaluation becomes costly when the full aerodynamic field contains a large number N_v of degrees of freedom. The unsteadiness of the coefficients is due to the velocity of the moving frame $\boldsymbol{s}_{\text{mfr}}(M,t) = \boldsymbol{s}_0(M_0,t) + \boldsymbol{\omega}(t)\wedge\widetilde{\boldsymbol{x}}_{\text{mfr}}(M)$ which produces the following expression of the linear non-autonomous coefficients

$$\begin{aligned}
\mathscr{L}^{\text{mfr}}_{ij}(t) &= \int_\Omega \left(\boldsymbol{s}_{\text{mfr}}(t)\cdot\nabla\varphi^{(j)}_\vartheta\right)\varphi^{(i)}_\vartheta\,\mathrm{d}\Omega \\
&+ \int_\Omega \left(\boldsymbol{s}_{\text{mfr}}(t)\cdot\nabla\varphi^{(j)}_{\boldsymbol{u}} - \boldsymbol{\omega}\wedge\varphi^{(j)}_{\boldsymbol{u}}\right)\cdot\varphi^{(i)}_{\boldsymbol{u}}\,\mathrm{d}\Omega \\
&+ \int_\Omega \left(\boldsymbol{s}_{\text{mfr}}(t)\cdot\nabla\varphi^{(j)}_p\right)\varphi^{(i)}_p\,\mathrm{d}\Omega.
\end{aligned} \tag{18}$$

The unsteady terms $\boldsymbol{s}_0(M_0,t)$ and $\boldsymbol{\omega}(t)$ can be extracted from the integrals in the previous expression since they do not depend on the position of the mesh points M. Using the properties of the triple product, the expression (18) is transformed into

$$\mathscr{L}^{\text{mfr}}_{ij}(t) = \boldsymbol{s}_0(t)\cdot\mathscr{L}^T_{ij} + \boldsymbol{\omega}(t)\cdot\mathscr{L}^R_{ij}, \tag{19}$$

where the new autonomous coefficients vectors $\mathscr{L}^T_{ij}$ and $\mathscr{L}^R_{ij}$ are respectively given by

$$\begin{aligned}
\mathscr{L}^T_{ij} &= \int_\Omega \varphi^{(i)}_\vartheta \nabla\varphi^{(j)}_\vartheta\,\mathrm{d}\Omega + \int_\Omega \varphi^{(i)}_p \nabla\varphi^{(j)}_p\,\mathrm{d}\Omega \\
&+ \int_\Omega \left[\left(\varphi^{(i)}_{\boldsymbol{u}}\right)^{\mathsf{T}}\nabla\varphi^{(j)}_{\boldsymbol{u}}\right]^{\mathsf{T}}\mathrm{d}\Omega
\end{aligned} \tag{20}$$

and

$$\begin{aligned}\mathscr{L}^R_{ij} &= \int_\Omega \left[\widetilde{\boldsymbol{x}}_{\text{mfr}} \wedge \nabla \boldsymbol{\varphi}^{(j)}_\vartheta\right] \boldsymbol{\varphi}^{(i)}_\vartheta \,\mathrm{d}\Omega \\ &+ \int_\Omega \left[\widetilde{\boldsymbol{x}}_{\text{mfr}} \wedge \nabla \boldsymbol{\varphi}^{(j)}_p\right] \boldsymbol{\varphi}^{(i)}_p \,\mathrm{d}\Omega \\ &+ \int_\Omega \widetilde{\boldsymbol{x}}_{\text{mfr}} \wedge \left[\left(\boldsymbol{\varphi}^{(i)}_{\boldsymbol{u}}\right)^{\mathsf{T}} \nabla \boldsymbol{\varphi}^{(j)}_{\boldsymbol{u}}\right]^{\mathsf{T}} \mathrm{d}\Omega \\ &- \int_\Omega \boldsymbol{\varphi}^{(j)}_{\boldsymbol{u}} \wedge \boldsymbol{\varphi}^{(i)}_{\boldsymbol{u}} \,\mathrm{d}\Omega\,.\end{aligned} \tag{21}$$

The constant non-autonomous terms $\mathscr{K}^{\text{mfr}}_i(t)$ are transformed in the same way. Each non-autonomous coefficient $\mathscr{K}^{\text{mfr}}_i(t)$ and $\mathscr{L}^{\text{mfr}}_{ij}(t)$ is now described by a set of two vectors which are multiplied by the translational and angular velocities of the domain. Consequently the number of non-autonomous coefficients is six times greater than before ($N^{\text{na}}_c = 6q + 6q^2$) but the coefficients can be computed once for all before the time integration of the reduced-order model. The reduced-order model is therefore described by $N_c = N^{\text{a}}_c + N^{\text{na}}_c$ constant coefficients. Details about the computation of the coefficients can be found in [53].

The computation of the surface contribution $\mathscr{Q}^D_{\text{Surf}}$ is based on the values of the POD modes, of the mean part and of the gradients on the domain boundaries. The values of the snapshots on the boundaries $\partial\Omega$ are also extracted here in such a way that the mean part and the POD modes on the boundaries can be computed with $\overline{\boldsymbol{q}}|_{\partial\Omega} = \sum_{m=1}^{M} \alpha_m \boldsymbol{q}^{(m)}|_{\partial\Omega}$ and $\boldsymbol{\varphi}^{(j)}|_{\partial\Omega} = \sum_{m=1}^{M} c^{(j)}_m (\boldsymbol{q}^{(m)}|_{\partial\Omega} - \overline{\boldsymbol{q}}|_{\partial\Omega})$. The gradient of the POD modes $\nabla\boldsymbol{\varphi}^{(j)}$ is computed in internal cells from the values of $\boldsymbol{\varphi}^{(j)}$ with a Finite Volume approximation in order to be consistent with the formalism used to obtain the snapshots. The evaluation of the gradients in the cells near the boundaries makes use of the values of the POD modes $\boldsymbol{\varphi}^{(j)}|_{\partial\Omega}$ computed on the boundaries and the values of $\nabla\boldsymbol{\varphi}^{(j)}|_{\partial\Omega}$ are extrapolated. It is thus recommended to store the values of the snapshots on the boundaries to improve the evaluation of the surface terms. Otherwise extrapolations are also needed to estimate $\overline{\boldsymbol{q}}|_{\partial\Omega}$ and $\boldsymbol{\varphi}^{(j)}|_{\partial\Omega}$.

To conclude this section on the construction of the POD-Galerkin reduced-order model, it should be mentioned that the model has been developed without the introduction of any artificial dissipation, whereas the classical Finite Elements or Finite Volume discretization methods generally make use of such procedures in order to stabilize the response for compressible flows. This is a potential source of instability which legitimates the need for a correction to improve the stability and the accuracy of the reduced-order model response.

3. Correction methods for POD-Galerkin reduced-order models of compressible flows

The reduced-order model is written in the compact form $\dot{\mathbf{a}} = \mathbf{f}^G(\mathbf{a},t)$ where $\mathbf{a} = [a_1,\ldots,a_q]^{\mathsf{T}}$ is the vector of the modal amplitudes and $\mathbf{f}^G(\mathbf{a},t)$ is a vector containing the polynomials $f^G_i(\mathbf{a},t)$ of the right hand size of equation (11), whose coefficients have been computed from the analytical expressions established in section 2. The objective of the correction methods is to determine the vector $\mathbf{f}^c(\mathbf{a},t)$ of the corrected polynomials such that the reduced-order model response is as close as possible to the one of the full-order model. Considering the sampling time interval $I_s = [t_0; t_0 + T_s]$, this means that the modal amplitudes $a_j(t_m)$ evaluated at the time instant t_m have

to coincide with the reference modal amplitudes $a_j^{(m)} = \langle \widetilde{\boldsymbol{q}}^{(m)}, \boldsymbol{\varphi}^{(j)} \rangle$ computed as the projection of the snapshots on the POD modes.

3.1. Calibration of the reduced-order model coefficients

This method used for example in [13, 18, 26, 27] relies on an optimization problem formulated for some coefficients of the polynomial vector $\mathbf{f}^G$, which are collected in the vector $\mathscr{X} \in \mathbb{R}^{p_c}$ where $p_c \leq N_c$. The corrected polynomial vector is therefore the solution of the optimization problem

$$\mathbf{f}^c = \mathbf{f}^G(\mathbf{a}, \mathscr{X}_{\text{opt}}) \quad \text{with} \quad \mathscr{X}_{\text{opt}} = \arg\min_{\mathscr{X} \in \mathbb{R}^{p_c}} \mathscr{J}(\varepsilon(\mathscr{X}, t)) \tag{22}$$

where the functional $\mathscr{J}$ to minimize is formulated for an error $\varepsilon(\mathscr{X}, t)$ which is defined as the difference between the modal amplitudes $\varepsilon_i(\mathscr{X}, t_m) = a_i^{(m)} - a_i(\mathscr{X}, t_m)$ or between the derivatives of the modal amplitudes $\varepsilon_i(\mathscr{X}, t_m) = \dot{a}_i^{(m)} - \dot{a}_i(\mathscr{X}, t_m)$. These two options are respectively the *state calibration* method and the *flow calibration* method according to [18]. The error can also be formulated for any physical quantity χ like the lift coefficient for example. In this case the correction is goal-oriented and the error is noted $\varepsilon_i(\mathscr{X}, t_m) = \chi_i^{(m)} - \chi_i(\mathscr{X}, t_m)$.

However the computation of the quantity χ induces high numerical costs when it involves the whole aerodynamic field. We therefore propose here a calibration based on the energetic content of each POD such that the error is defined by $\varepsilon_i(\mathscr{X}, t) = \lambda_i - E[a_i(\mathscr{X}, t) a_i(\mathscr{X}, t)]$ and the functional to minimize is $\mathscr{J}(\varepsilon(\mathscr{X}, t)) = \sum_{i=1}^{q} |\varepsilon_i(\mathscr{X}, t)|^2$. This formulation can be viewed as the calibration of an 'energy' $\mathscr{E}_T^*$ similar to the total energy $\mathscr{E}_T$ of the dynamical system. Indeed, the average of the quantity $\mathscr{E}_T^* = \langle \boldsymbol{q}, \boldsymbol{q} \rangle = \int_\Omega (\vartheta^2 + \boldsymbol{u}^\mathsf{T}\boldsymbol{u} + p^2) \mathrm{d}\Omega$ is $E[\mathscr{E}_T^*] \approx \sum_{i=1}^{q} \lambda_i$. For compressible flows, the energy $\mathscr{E}_T^*$ is not exactly the total energy but numerical results reveal that the calibration of $\mathscr{E}_T^*$ provides the same correction as if the coefficients were calibrated with the real physical total energy $\mathscr{E}_T$ [53]. For incompressible fluids, the energy $\mathscr{E}_T^* = \langle \boldsymbol{q}, \boldsymbol{q} \rangle$ represents twice the kinetic energy per unit mass of the system and such a calibration has therefore a physical meaning.

Finally the functional to minimize is formulated for the average norm of the error

$$\mathscr{J}(\varepsilon(\mathscr{X}, t)) = E\left[\|\varepsilon(\mathscr{X}, t)\|_2^2 \right] = \sum_{m=1}^{M} \alpha_m \sum_{i=1}^{N_{\text{dofs}}} |\varepsilon_i(\mathscr{X}, t_m)|^2 \tag{23}$$

where the number N_{dofs} is equal to q if the error is based on the (derivatives of the) modal amplitudes and to 1 if a scalar quantity like the energy is considered. Since the functional $\mathscr{J}(\varepsilon(\mathscr{X}, t))$ is highly nonlinear, the optimal solution is computed with the Levenberg-Marquardt algorithm [25].

3.2. Identification of the reduced-order model coefficients

The nonlinear dependency of the functional can be simplified by the linearization of the problem where the modal amplitudes are approximated by $\mathbf{a}(\mathscr{X}, t_m) \approx \mathbf{a}^{(0)} + \int_{t_0}^{t_0 + t_m} \mathbf{f}^G(\mathbf{a}^{(m)}(\tau), \mathscr{X}) \mathrm{d}\tau$ for the state calibration and by $\dot{\mathbf{a}}(\mathscr{X}, t_m) \approx \mathbf{f}^G(\mathbf{a}^{(m)}, \mathscr{X})$ for the flow calibration. The optimization problem becomes a linear least-squares problem which is generally ill-posed. Couplet et al. [18] therefore introduced a regularization term to solve the problem but the determination of the regularization parameter is not obvious. Recently, a Tikhonov regularization of the problem has

been introduced [17, 51, 66] to determine properly this parameter by means of the L-curve method introduced in [32].

Since the reference modal amplitudes $\mathbf{a}^{(m)}$ should be governed by the set of ordinary differential equations of the reduced-order model, the equalities (11) should be satisfied for each amplitude and at each time instant t_m. These equations correspond to $\dot{\mathbf{a}}(\mathscr{X},t_m) \approx \mathbf{f}^G(\mathbf{a}^{(m)},\mathscr{X})$ and write for each amplitude $\dot{a}_i^{(m)}$ under the matrix form

$$\mathscr{A}\,\mathscr{X}_i = \mathscr{B}_i, \tag{24}$$

where $\mathscr{B}_i = [\dot{a}_i^{(1)} \cdots \dot{a}_i^{(M)}]$, $\mathscr{X}_i = [\mathscr{X}_i^{\mathrm{a}}\ \mathscr{X}_i^{\mathrm{na}}]^{\mathsf{T}}$ is the vector containing the unknown coefficients for the autonomous and non-autonomous parts such that

$$\begin{aligned} \mathscr{X}_i^{\mathrm{a}} &= \left[\ \mathscr{K}_i \ \cdots\ \mathscr{L}_{ij}\ \cdots\ \mathscr{Q}_{ijk,k\geq j}\ \cdots\ \right]^{\mathsf{T}} \\ \mathscr{X}_i^{\mathrm{na}} &= \left[\left(\mathscr{K}_i^T\right)^{\mathsf{T}}\left(\mathscr{K}_i^R\right)^{\mathsf{T}}\cdots\left(\mathscr{L}_{ij}^T\right)^{\mathsf{T}}\cdots\left(\mathscr{L}_{ij}^R\right)^{\mathsf{T}}\cdots\right]^{\mathsf{T}}, \end{aligned} \tag{25}$$

and $\mathscr{A} = [\mathscr{A}^{\mathrm{a}}\ \mathscr{A}^{\mathrm{na}}]$ is a matrix containing the correlations of the amplitudes associated to the coefficients of $\mathscr{X}_i$. The system (24) is generally ill-posed and the matrix $\mathscr{A}$ is often ill-conditioned. An approximate solution $\widetilde{\mathscr{X}}_i$ can however be looked for. Two regularization techniques are used in this paper. The first one is based on the Tikhonov regularization and the approximated solution of the problem is

$$\widetilde{\mathscr{X}}_i = \arg\min_{\mathscr{X}\in\mathbb{R}^{N_c}} \|\mathscr{A}\,\mathscr{X} - \mathscr{B}_i\|_2^2 + \lambda_{\mathrm{Tikh}}\|\mathscr{X} - \mathscr{X}_0\|_2^2, \tag{26}$$

where λ_{Tikh} is the regularization parameter computed by the L-curve method [32] and $\mathscr{X}_0$ is an initial guess of the coefficients which are here computed by the analytical expressions given in section 2.2.

An alternative solution is to compute the pseudo-inverse of the matrix $\mathscr{A}$ by means of a singular value decomposition and to truncate the decomposition to eliminate the smallest singular values. The pseudo-inverse $\mathscr{A}_p^+$ evaluated with the first p singular values is then used to obtain the approximated solution

$$\widetilde{\mathscr{X}}_i = \mathscr{A}_p^+\,\mathscr{B}_i. \tag{27}$$

The order of truncation can also be determined with the L-curve method. Unlike the Tikhonov regularization method, there is no use of the initial guess $\mathscr{X}_0$ and the solution is possibly very far from the values given by the analytical expressions derived with the Galerkin projection.

4. Reduced-order model of the flow field around a fixed NACA0012 airfoil

4.1. Generation of the snapshots database

A reduced-order model is first constructed to reproduce the vortex shedding process emerging in the wake of a NACA0012 airfoil. The Navier-Stokes equations including the viscous terms have thus to be considered since the vortex shedding is mainly due to viscous processes. The flow parameters are $\mathrm{Re} = 2\,000$ and $\mathrm{Ma} = 0.2$ and the angle of attack of the profile is $\alpha = 20^\circ$.

The vortex shedding process has been extensively studied by Pulliam [55] on the interval $\mathrm{Re} \in [800; 3\,000]$ and POD-Galerkin reduced-order models have already been constructed for the same configuration [12, 39, 64]. For this configuration the flow is two-dimensional and a 2D C-shape spatial domain is therefore used. The mesh generated with a transfinite interpolation method is composed of $N = 19\,100$ discretization control cells and the number of degrees of freedom of the full-order model reaches $N_v = 76\,400$.

Since the computation of the POD modes requires the generation of a snapshots database, a simulation is first performed with the full-order model. The result of a steady computation with the Finite Volume solver *elsA* [28] is shown on figure 1(a). The existence of a recirculation zone is a clue of the emergence of the vortex street. The vortex shedding process is captured with an unsteady computation performed with a two-level multigrid method and a backward Euler scheme for the time integration. The periodic vortex shedding creates an oscillation of the lift coefficient which is represented on figure 1(b). The Fourier transform of the lift coefficient produces a peak corresponding to the dimensionless Strouhal period $T^*_{\mathrm{St}} = 9.6$.

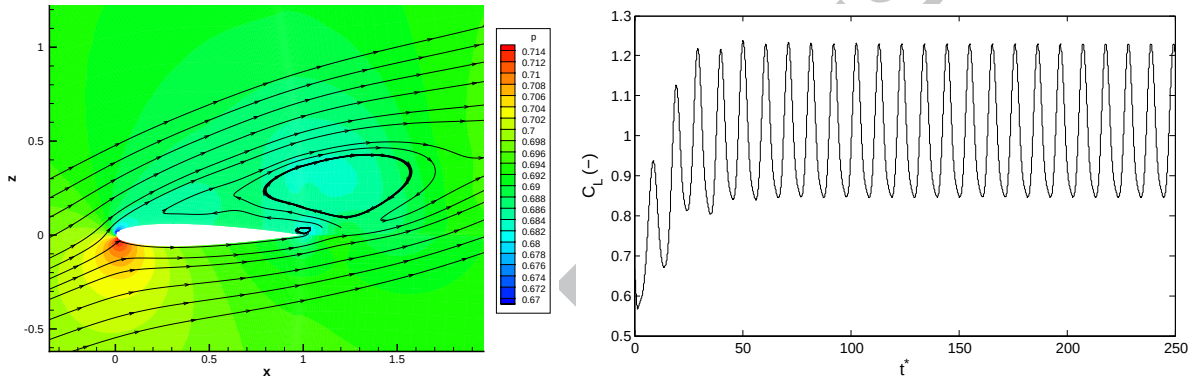

(a) Steady dimensionless pressure field

(b) Oscillations of the lift coefficient

Figure 1: Representation of the steady pressure field and of streamlines around the NACA0012 airfoil (a) and plot of the oscillations of the lift coefficient produced by the periodic vortex shedding process (b).

4.2. Computation of the POD modes

A set of M dimensionless snapshots is extracted on the sampling time interval I_s. The extraction is performed regularly with the time step δt_c over about one and a half Strouhal period. The POD modes and eigenvalues are first computed with the snapshots method [61] which is here considered to be the reference solution. Figure 2 represents the percentage of energy $\widetilde{\eta}_i = \lambda_i / \sum_{j=1}^{r} \lambda_j$ captured by each POD mode. This quantity is compared when the eigenvalues are computed with the method of Chahlaoui et al. [16] which provides a recursive approximation of the dominant singular subspace. The circles are the reference eigenvalues λ_i computed with the snapshots method. The red squares are the converged singular values σ_i^2 for $i = 1, \ldots, q$ and the empty squares detail the convergence of each singular value. The asterisks represent the dismissed singular values σ_i^2 for $i = q+1, \ldots, M$. The graph has been plotted for $M = 50$ snapshots and the dimension of the approximated subspace is $q = 20$. Since the whole snapshots matrix cannot be stored in memory,

the algorithm begins with the QR decomposition of the truncated snapshots matrix containing only the first q snapshots. This first approximation is then enriched by the $M-q$ missing snapshots to get finally an accurate estimation of the left singular subspace and of the singular values.

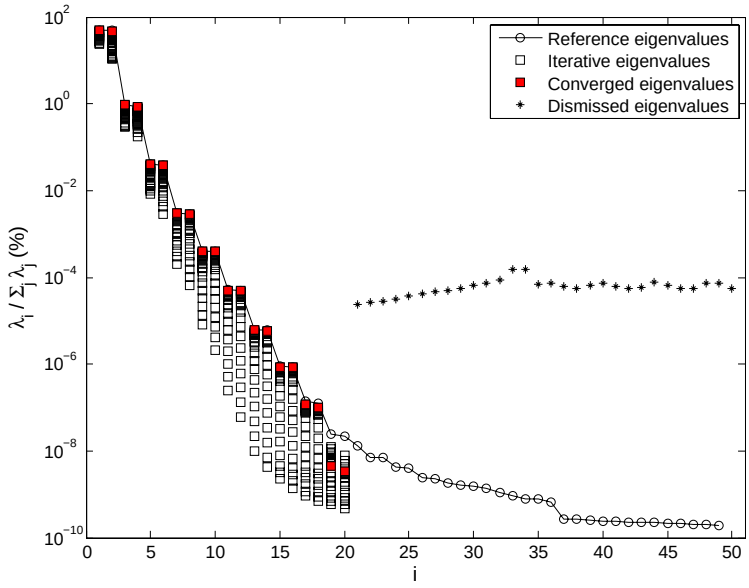

Figure 2: Spectrum of the eigenvalues associated to the POD modes. The reference curve (○) is the spectrum computed with the snapshots method, whereas the spectrum computed with the iterative QR decomposition [16] is represented by the red squares (■) for the converged values. The dismissed eigenvalues are given by the asterisks (∗).

The eigenvalues are grouped by pairs as usually for flows exhibiting a vortex shedding process [17, 39, 40, 60]. The first POD modes capture almost all of the energy of the system: with $M = 50$ snapshots used to compute the POD modes, the truncation error $\varepsilon_q = \sum_{j=q+1}^{r} \lambda_j / \sum_{j=1}^{r} \lambda_j$ is about 1.2e-4 % when the projection basis contains only $q = 10$ POD modes.

The eigenvalues computed by both methods compare well. The error $|\lambda_i - \sigma_i^2|/|\lambda_i|$ is given in Table 1 for the first ten eigenvalues. The error is larger for the last eigenvalues and the precision increases for these eigenvalues as the dimension of the subspace q increases. The computation costs of the iterative QR decomposition are much smaller. The graph on figure 3 compares the CPU times necessary to compute the POD modes for different sizes of the snapshots database. The CPU time increases with the square of M for the snapshots method whereas it grows linearly for the QR decomposition. Indeed, in the first case the snapshots have to be read $M(M+1)/2$ times to compute each term of the symmetric covariance matrix $\mathbf{R}^\star$ while only M readings of the snapshots are needed to approximate the subspace in the second case.

The pattern of the POD modes is represented on the figure 4. On each line, the pressure part of the POD mode $\varphi_p^{(i)}$ for $i = 1, \ldots, 4$ is shown. In the first three columns, the POD modes have been computed with the iterative QR decomposition when the size of the POD basis is $q = 5$, 10 or 30. In the last column, the POD modes come from the resolution of the eigenvalue problem (5) with the snapshots method. The structure of the POD modes is practically the same with the iterative QR decomposition method, whatever the dimension q of the approximated subspace.

$q = 5$	$q = 10$	$q = 20$	$q = 30$
0.06	0.06	0.06	0.06
3.71	3.71	3.71	3.71
0.86	0.82	0.82	0.82
3.20	3.18	3.18	3.18
11.9	2.18	2.18	2.18
–	1.51	1.50	1.50
–	3.38	2.03	2.03
–	1.32	0.62	0.62
–	56.3	2.71	2.71
–	94.7	0.30	0.30

Table 1: Relative error (in percentage) for the first ten POD eigenvalues computed for different dimensions q of the POD subspace.

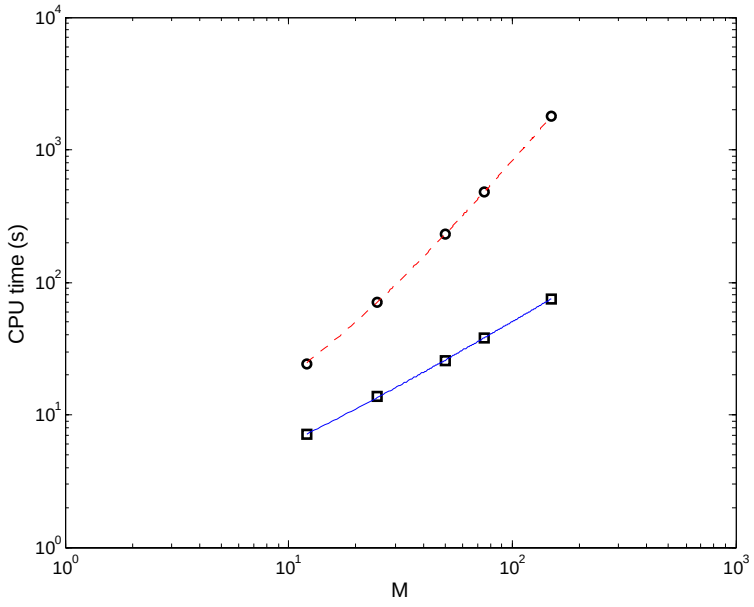

Figure 3: Comparison of the CPU times for the computation of the POD modes with the snapshots method (○) and the iterative QR decomposition (□). The continuous (—) and dashed (– –) curves are first and second order polynomial approximations.

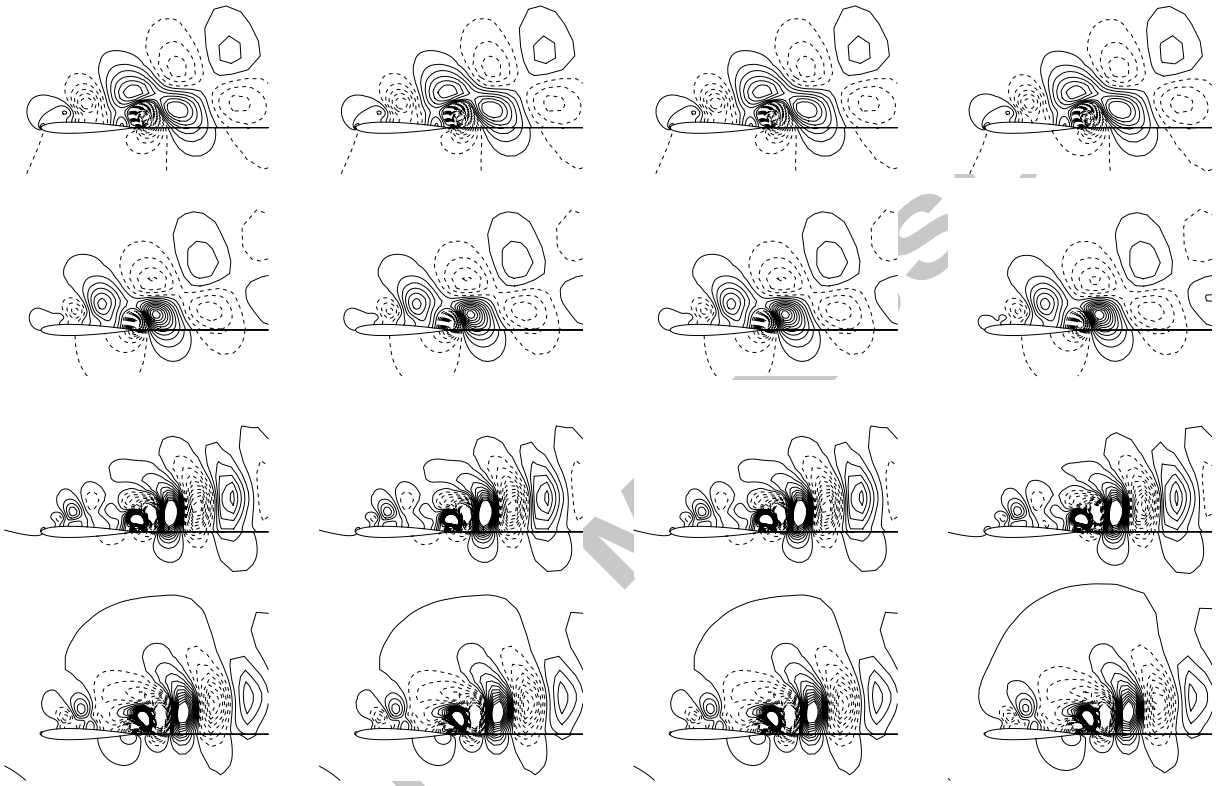

(a) $q = 5$ (b) $q = 10$ (c) $q = 30$ (d) Reference

Figure 4: Comparison of the pressure part $\varphi_p^{(i)}$ of the POD modes computed by different ways. Each row represents respectively the first, second, third and fourth POD modes computed with the iterative QR decomposition method [16] with (a) $q = 5$, (b) $q = 10$ or (c) $q = 30$ and (d) with the snapshots method [61] used here as a reference. The continuous (resp. dashed) lines represent positive (resp. negative) isovalues.

Finally the convergence of the proper orthogonal decomposition approximation is checked on the figure 5(a) when the number of snapshots M or the number of POD modes q is increased. For that purpose, the reference snapshots $\boldsymbol{q}^{(m)}$ are reconstructed by the decomposition (2) using the POD modes computed from the snapshots database containing M snapshots and a projection basis with q POD modes. The aerodynamic field reconstructed in this way is $\boldsymbol{q}_{\text{POD}}^{(m)} = \overline{\boldsymbol{q}} + \sum_{j=1}^{q} a_j^{(m)} \boldsymbol{\varphi}^{(j)}$ where the coefficients $a_j^{(m)} = \langle \boldsymbol{q}^{(m)}, \boldsymbol{\varphi}^{(j)} \rangle$ are the reference modal amplitudes. The reconstruction error is defined for the snapshots by $\varepsilon_{L^2,\boldsymbol{q}} = ||\boldsymbol{q}^{(m)} - \boldsymbol{q}_{\text{POD}}^{(m)}||_{L^2} / ||\boldsymbol{q}^{(m)}||_{L^2}$ at each time instant t_m with the definition (1) for the L^2 norm. Then the time average error $E[\varepsilon_{L^2,\boldsymbol{q}}]$ is plotted on figure 5(a) with a logarithmic scale. There is clearly a convergence when the number of POD modes is increased but the influence of the number of snapshots is not significant. The reconstruction error is very small and converges but in this case the modal amplitudes have been obtained by the projection of the snapshots on the POD basis. In the next section, the same error is evaluated when the modal amplitudes are computed from the resolution of the reduced-order model.

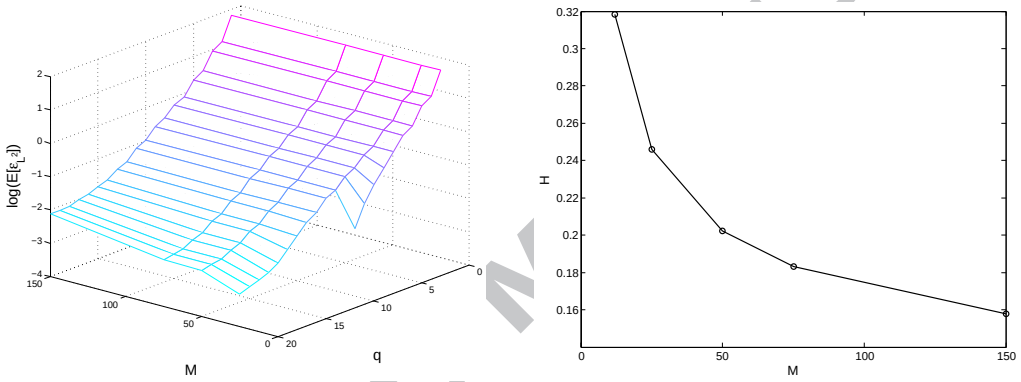

(a) Convergence of the reconstruction error (b) Convergence of the entropy

Figure 5: Convergence of the reconstruction error $E\left[\varepsilon_{L^2,\boldsymbol{q}}\right]$ when the number M of snapshots and the number q of POD modes used in the proper orthogonal decomposition is increased (a). When the number of snapshots used to compute the POD modes is increased, the entropy H of the system converges (b).

The influence of the number of snapshots is highlighted on figure 5(b) by the graph of the system entropy defined by

$$H = -\lim_{M\to\infty} \frac{1}{\log M} \sum_{m=1}^{M} \widetilde{\eta}_m \log \widetilde{\eta}_m \quad \text{with} \quad \widetilde{\eta}_m = \frac{\lambda_m}{\sum_{j=1}^{r} \lambda_j}. \tag{28}$$

Although the influence of the number of snapshots is not significant for the reconstruction error, it has a great influence on the value of the system entropy. Increasing the number of snapshots seems to provide a better description of the system whose entropy converges. Since the entropy is a measure of the system disorder, the low limit value $H < 0.16$ indicates that the system energy is concentrated on the first eigenvalues. This justifies the construction of a reduced-order model with only the first POD modes.

4.3. Evaluation of the reduced-order model response

The previous results have demonstrated the ability of the POD modes to represent the snapshots database. Now the reduced-order model is constructed and the modal amplitudes are computed as the solution of the system of ordinary differential equations (11) to reproduce the aerodynamic field. Since the structure is fixed, the system is just described by the autonomous operators $\mathscr{K}$, $\mathscr{L}$ and $\mathscr{Q}$. The coefficients of the reduced-order model are computed for $q = 10$ POD modes and $M = 50$ snapshots. The reduced-order model is initialized with the modal amplitudes $a_i(t_0) = \langle \boldsymbol{q}^{(1)}, \boldsymbol{\varphi}^{(i)} \rangle$ corresponding to the first snapshot. Since the system is autonomous, other initial conditions could be determined with the shooting method of Akhtar et al. [2] and may improve the accuracy of the limit-cycle on which the system converges. The time integration is performed on the sampling time interval I_s so that the solution can be compared to the reference solution given by the snapshots. Since the reduced-order model (11) is defined by a set of explicit ordinary differential equations, its integration in time is performed with classical procedures. The `lsoda` solver of the package `ODEPACK` [36] adopted here automatically chooses according to the stiffness of the problem between a predictor-corrector Adams scheme or the Backward Differentiation Formula.

The result is plotted on figure 6 where the trajectories of the modal amplitudes computed by the reduced-order model are compared to those of reference. The limit cycles are not well reproduced and clearly reveal a lack of dissipation in the response which tends to diverge as the time integration is pursued. The relative error $\overline{\varepsilon_{a_j}}$ plotted for each modal amplitude on the last graph of figure 6 is defined by $\overline{\varepsilon_{a_j}} = 100\,||a_j^{(m)} - a_j(t_m)||_{L^2(I_s)} / ||a_j^{(m)}||_{L^2(I_s)}$ where $||x(t)||_{L^2(I_s)} = (\int_{t_0}^{t_0+T_s} x^2(t)\,\mathrm{d}t)^{1/2}$. This error is relatively small for the first amplitudes (about 25%) but increases significantly for the last ones whose values are about 500%. However, the global response of the dynamical system is mainly characterized by the first modal amplitudes and consequently the macroscopic quantities are qualitatively well reproduced. The lift coefficient is plotted on figure 7(a) over a longer time interval. Over the sampling time interval I_s delimited by the black rectangle, the lift coefficient is rather well reproduced ($\overline{\varepsilon_{C_L}} = 3.8\%$) even if the errors $\overline{\varepsilon_{a_j}}$ on the modal amplitudes are significant. The relative error on the frequency is only 1.5% and the physics of the vortex shedding is well reproduced. Although the results of figure 6 showed a potential divergence, a saturation of the oscillations is observed and the response is stable for long time integration. However the lack of dissipation induces an over-estimation of the amplitude of oscillation for the lift coefficient and a correction of the reduced-order model is necessary.

The error is not reduced by the introduction of more POD modes or snapshots in the database as shown on figure 7(b). Unlike the plot of figure 5(a), the error reaches an asymptotic value as soon as $q = 10$ POD modes are kept in the projection basis. Although the introduction of new POD modes reduces continuously the approximation error of the snapshots with the proper orthogonal decomposition using the reference modal amplitudes $a_j^{(m)}$, this is no longer the case when the modal amplitudes are computed by the reduced-order model when $q > 10$.

4.4. Improvement of the reduced-order model response

As stated in the introduction, many corrections methods could be considered to improve the stability. The modification of the initial conditions by the shooting method suggested in [2] could

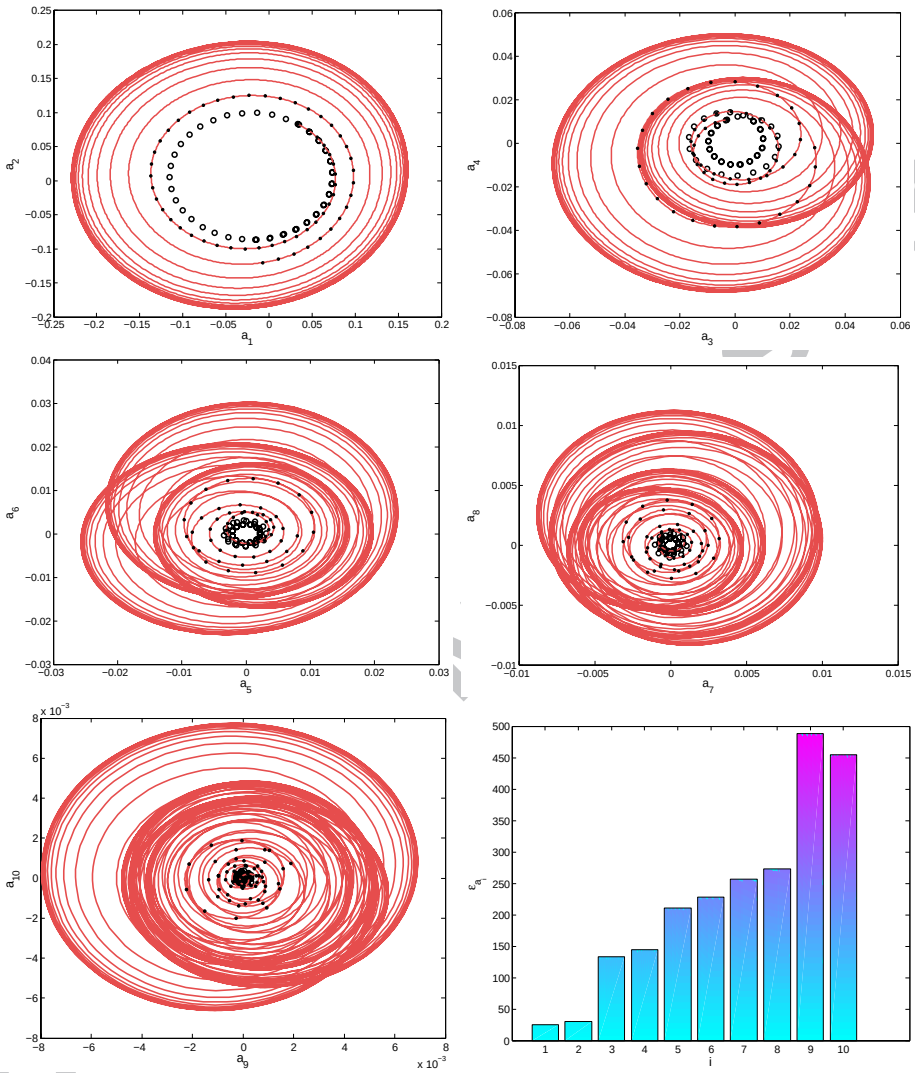

Figure 6: Comparison of the trajectories of the modal amplitudes $\{a_j(t)\}_{j=1}^{10}$ computed with the reduced-order model on short- (●) or long-term (—) and of the modal amplitudes of reference $a_j^{(m)}$ obtained by the projection of the snapshots (○). The last graph represents the relative time averaged error $\overline{\varepsilon_{a_j}}$.

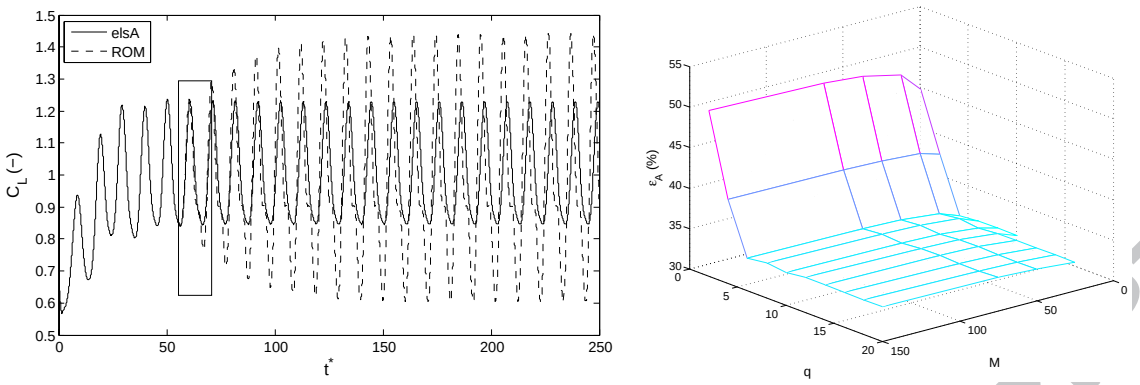

(a) Evolution of the lift coefficient (b) Convergence of the modal amplitudes

Figure 7: Comparison of the lift coefficient of reference computed with the full-order model to the one reproduced by the reduced-order model over several Strouhal periods (a). The convergence of the infinite error for the modal amplitudes is represented on the graph (b) when the number of snapshots and POD modes is increased.

be useful in this case since the reduced-order model is autonomous. However, since we are later interested in non-autonomous systems, we rather consider the correction methods described in section 3.2. The nonlinear optimization problem (22) is solved for different types of errors $\varepsilon(\mathscr{X},t)$ based on the modal amplitudes (state calibration) or on the energy $\mathscr{E}_T^*$ captured by each POD mode. Different sets of coefficients to optimize have also been investigated. The combinations of errors and parameters are given in Table 2 according to the number p_c of coefficients to calibrate.

The calibration called `qRe` consists in finding the best corrected Reynolds numbers Re_i associated to each equation of the reduced-order model and thus operates on the linear diagonal terms. A better correction is obtained when the constant and linear diagonal terms are optimized. This calibration called `KdL` does not only modify the diffusive contribution of the linear term but operates on the global linear diagonal term. Likewise, the calibration `KL` provides optimal values for the constant and linear operators. See [29, 53] for a thorough comparison between the different correction methods and a discussion on the initialization of the optimization algorithm.

Table 2: Parameters of the optimization problem for the calibration of the reduced-order model.

Identifier	$\varepsilon_i(\mathscr{X},t_m)$	Coeff.	p_c
`qRe - State`	$a_i^{(m)} - a_i(\mathscr{X},t_m)$	Re_i	q
`qRe - Energ.`	$\lambda_i - E[a_i(\mathscr{X},t_m)a_i(\mathscr{X},t_m)]$	Re_i	q
`KdL`	$a_i^{(m)} - a_i(\mathscr{X},t_m)$	$\mathscr{K}_i, \mathscr{L}_{ii}$	$2q$
`KL`	$a_i^{(m)} - a_i(\mathscr{X},t_m)$	$\mathscr{K}_i, \mathscr{L}_{ij}$	$q+q^2$

The lift coefficient computed with the reduced-order model is compared on figure 8 to the reference response of the full-order model. On the first period, the different calibrations perform well and the response is very accurate. However, discrepancies appear on the long-term. The am-

plitude of oscillation is well captured but a phase-lag is clearly visible on the twenty-fifth period. The calibration of the Reynolds numbers with the state or energetic approaches produces nearly the same results although two different quantities have been minimized. The relative error on the frequency is 1.4% with the calibrations `qRe`, 1.0% with the calibration `KdL` and drops to 0.1% with the calibration `KL`. The solution is improved when the number of calibrated coefficients increases. Indeed, the calibration of the constant and linear diagonal terms (`KdL`) or the calibration of the constant and all the linear terms (`KL`) improves further the estimation of the frequency.

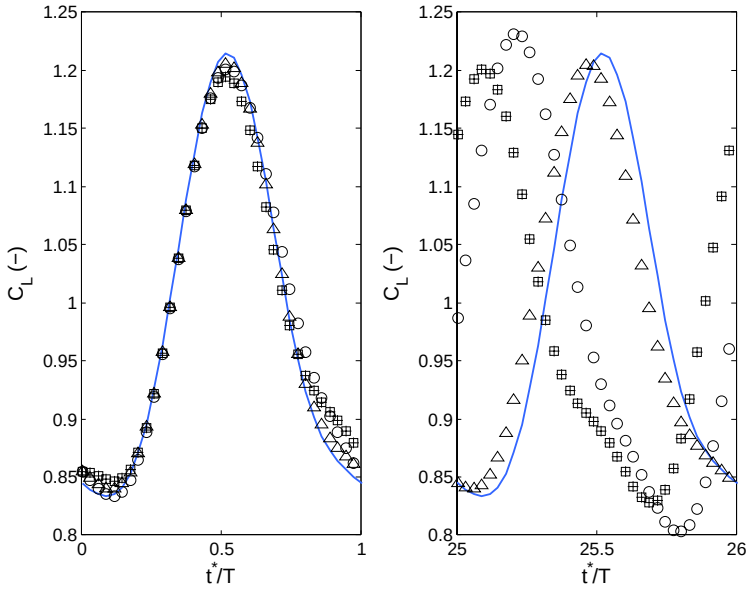

Figure 8: Comparison of the lift coefficient computed with the reduced-order model calibrated with the different combinations given in table 2: (+) `qRe` - state calibration, (□) `qRe` - energetic calibration, (○) `KdL`, (△) `KL`. The lift is compared on the 1st and 25th period of oscillation to the reference response (—) computed with the full-order model.

The accuracy of each calibration is evaluated on the short-term response where the snapshots are known. The relative error on the lift coefficient computed with the state or energetic calibration `qRe` of the Reynolds numbers is respectively $\overline{\varepsilon_{C_L}} = 2.14\%$ and $\overline{\varepsilon_{C_L}} = 2.12\%$. Then the error drops at $\overline{\varepsilon_{C_L}} = 1.67\%$ for `KdL` and $\overline{\varepsilon_{C_L}} = 1.52\%$ for `KL`. The errors on each modal amplitude are represented on figure 9. The accuracy is much better when all the linear coefficients are calibrated. The accuracy is the most important for the first amplitudes which mainly govern the response, but since the system is nonlinear an error on the last amplitudes is able to destabilize the response and the error should also be reduced for these amplitudes.

In this section a reduced-order model for the Navier-Stokes equations of the flow around a fixed structure has been constructed using an original algorithm to compute the POD modes and adequate calibrations methods have been investigated to reproduce correctly the limit-cycle oscillations of the lift coefficient. Numerical results show that the calibration of constant and linear diagonal coefficients provides an enough accurate solution in terms of stability and amplitude and frequency of oscillation. An even better solution can be reached with the calibration of all the linear coefficients after the resolution of a more demanding optimization problem. The objective

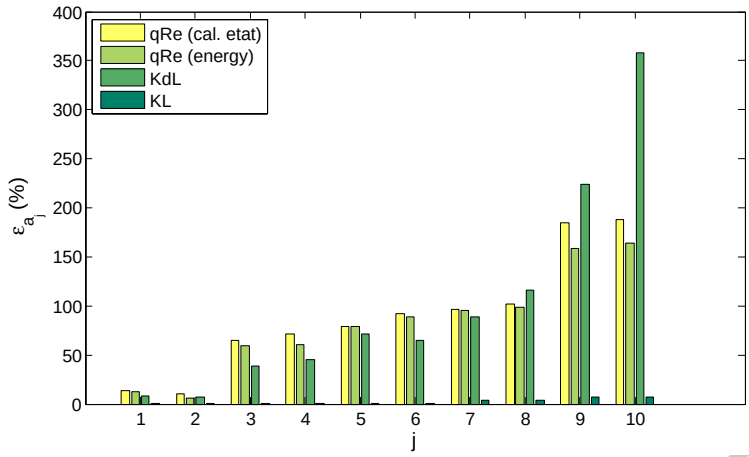

Figure 9: Comparison of the error $\overline{\varepsilon_{a_j}}$ for the modal amplitudes computed as the solution of the reduced-order model corrected for the set of coefficients `qRe`, `KdL` and `KL`. The error relative to the calibration of the energetic content $\mathscr{E}_T^*$ is also given for the set of coefficients `qRe`.

of the next section is to evaluate the formulation of the reduced-order model developed in this paper to take into account the motion of a structure and to investigate the potential of the correction methods used previously in the case of a fixed structure.

5. Reduced-order model of the flow field around an oscillating NACA0064 airfoil

5.1. Generation of the snapshots database

The second reduced-order model is developed to reproduce the shock oscillation induced by the motion of a NACA0064 airfoil in a transonic flow at $\mathrm{Ma}_\infty = 0.796$. In this case the Euler equations are considered since the viscous processes are not of prime importance. A 2D C-shape spatial domain containing $N = 8\,192$ discretization control cells is used and the number of degrees of freedom of the full-order model is $N_v = 32\,768$.

The airfoil is subjected to a translational motion at a constant horizontal velocity V_∞ and a rotation is prescribed via the pitch angle α which oscillates at the frequency ω_α. The rotational motion is therefore described by $\alpha(t) = \alpha_m \sin(\omega_\alpha t)$, where $\alpha_m = 1.0$. The translational velocity $\boldsymbol{s}_{\mathrm{mfr}}$ and the angular velocity $\boldsymbol{\omega}$ of the moving frame thus write

$$\boldsymbol{s}_{\mathrm{mfr}} = V_\infty \begin{bmatrix} \cos\alpha(t) \\ 0 \\ \sin\alpha(t) \end{bmatrix} \quad \text{and} \quad \boldsymbol{\omega} = \begin{bmatrix} 0 \\ \dot{\alpha}(t) \\ 0 \end{bmatrix}. \tag{29}$$

The result of a steady computation conducted in the relative frame of reference with $\alpha = 0$ is shown on figure 10. Two shock waves are revealed on each side of the airfoil at the same position on the chord since the angle of attack is null. When the pitch angle oscillates with a prescribed motion, the position of the shock waves oscillates in opposite direction on each side of the profile.

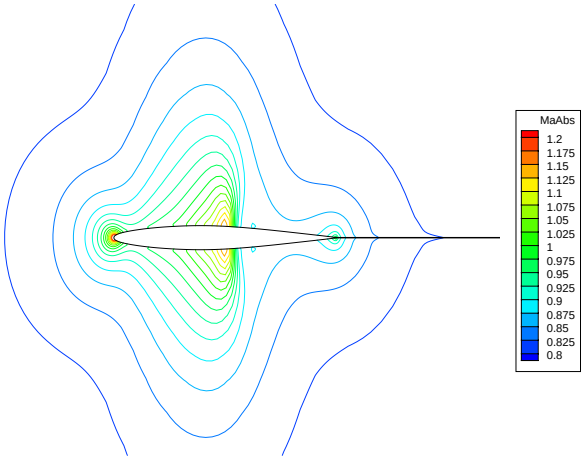

Figure 10: Isovalues of the steady Mach number around the NACA0064 airfoil. The angle of attack is set to $\alpha = 0$.

Unsteady computations are then performed with a prescribed motion on several periods to reach the convergence. The simulation is initialized with the aerodynamic field presented on figure 10 since at $t = 0$ the angle of attack is null.

5.2. Computation of the POD modes

A set of $M = 120$ dimensionless snapshots is extracted regularly on the sampling time interval I_s covering about two and a half period selected after the transient has vanished. A longer time interval was selected here since the stability of the reduced-order model proved to be better in this case. Figure 11 represents the percentage of energy $\widetilde{\eta}_i = \lambda_i / \sum_{j=1}^{r} \lambda_j$ captured by each POD mode for a basis containing $q = 30$ modes. The converged values computed with the method of Chahlaoui et al. [16] compare well to those computed with the classical snapshots method like in the case of the fixed NACA0012 airfoil.

The eigenvalues are no longer grouped by pairs and the slope is less pronounced than in the previous example. However the first POD modes contain most of the system energy since the truncation error ε_q is about 4.2e-3 % when the projection basis contains only $q = 10$ POD modes.

The structure of the first six POD modes is represented on figure 12. The POD modes have been computed from a subspace approximation with $q = 30$ snapshots and then completed with the $M - q = 90$ remaining snapshots. There is no visible difference with POD modes computed with the classical snapshots method (not shown on Fig. 12). The POD modes exhibit the oscillating pattern of the shock which is decomposed in several discontinuous areas along the airfoil chord. The POD modes are no longer grouped by pairs but several structures are common to two consecutive modes : modes 1 and 2 are characterized by only one large shock structure on each side of the airfoil, whereas the next modes are composed of two or three similar structures of lower spatial extent. The entropy is $H = 0.15$ for $M = 120$ and decreases very slightly when the number of snapshots is increased further. Consequently, a reduced-order model based on the first most energetic POD modes should here again be able to represent the physics of the shock oscillation.

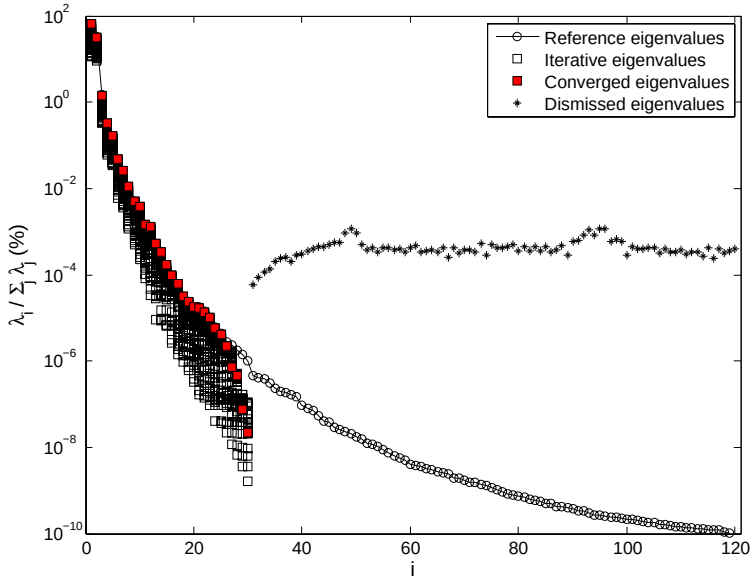

Figure 11: Spectrum of the POD eigenvalues computed with the iterative QR decomposition [16] involving initially $q = 30$ snapshots. The reference curve in black (—) is the spectrum computed with the snapshots method.

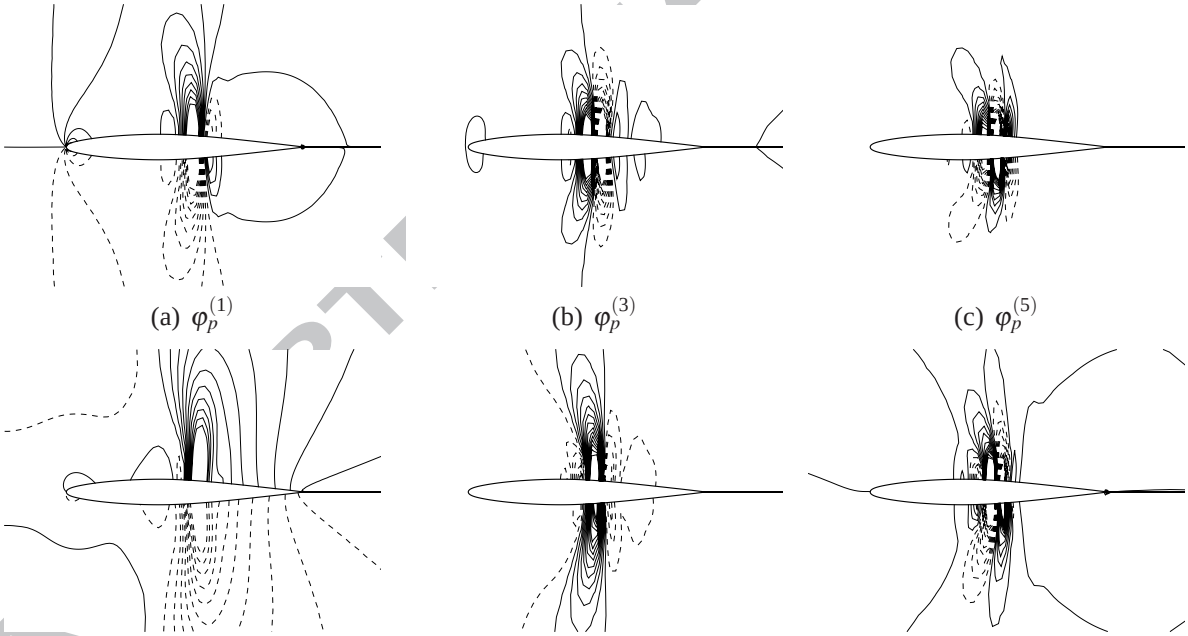

Figure 12: Pressure part $\varphi_p^{(i)}$ of the first six POD modes computed for the oscillating NACA0064 airfoil with the iterative QR decomposition method [16] with $M = 120$ snapshots. The continuous (resp. dashed) lines represent positive (resp. negative) isovalues.

5.3. Evaluation of the reduced-order model response

The reduced-order model described by Eq. (11) involves now autonomous and non-autonomous terms. The coefficients associated to these terms are now computed from the set of snapshots $\boldsymbol{q} = [\vartheta, \boldsymbol{u}, p]^{\mathsf{T}}$, where the velocity vector is defined in the relative frame of reference attached to the rigid body motion of the structure. The non-autonomous terms $\mathscr{K}_i^{\text{mfr}}(t)$ and $\mathscr{L}_{ij}^{\text{mfr}}(t)$ which describe the motion of the spatial domains are defined by Eqs. (19), (20) and (21) in the general case but since the rigid body motion is only made up of a translation and a rotation, the non-autonomous reduced-order model coefficients write

$$\mathscr{L}_{ij}^{T} = \begin{bmatrix} \mathscr{L}_{ij,x}^{T} \\ 0 \\ \mathscr{L}_{ij,z}^{T} \end{bmatrix} \quad \text{and} \quad \mathscr{L}_{ij}^{R} = \begin{bmatrix} 0 \\ \mathscr{L}_{ij,y}^{R} \\ 0 \end{bmatrix} \tag{30}$$

according to the definition Eq. (29) of the translational and angular velocities. Due to the previous simplification, the number of non-autonomous coefficients is now $N_c^{\text{na}} = 3q + 3q^2$.

The reduced-order model constructed for this new system is very unstable, even if the number of POD modes used in the projection basis and the number of snapshots included in the database is increased. This may be attributed to the absence of any dissipation in the reduced-order model, which is crucial for transonic flows. Indeed, the Euler equations have been here projected without introducing some numerical dissipation to stabilize the response, although such a procedure is used in the full-order model. The calibration techniques presented in section 3.1 could therefore be used to account for this numerical dissipation.

The calibration called `qRe` in table 2, which modifies the Reynolds number for each equation of the reduced-order model, cannot be used in this case because of the absence of any diffusive term. The sets of calibrated coefficients `KdL` and `KL` which yielded previously satisfactory results do no longer provide an adequate correction since the reduced-order model response diverges rapidly from the lift limit-cycle obtained with the full-order model. The sole calibration of autonomous constant and linear coefficients is not sufficient in the present case. Consequently, a new set of coefficients called `KdL_mfr` has been employed to improve also the coefficients associated to the non-autonomous terms.

Instead of optimizing all the non-autonomous constant and linear coefficients $\mathscr{K}_i^T$, $\mathscr{K}_i^R$, $\mathscr{L}_{ij}^T$ and $\mathscr{L}_{ij}^R$, the calibration termed `KdL_mfr` is acting on the translational and angular velocities $\boldsymbol{s}_{\text{mfr}}$ and $\boldsymbol{\omega}$ from which the non-autonomous coefficients are defined by Eq. (19). In this way, only 6 additional coefficients (instead of $N_c^{\text{na}} = 3q + 3q^2$) have to be determined and the calibration `KdL_mfr` optimizes finally $2q + 6$ coefficients.

The results of the time integration of the reduced-order model built with $q = 10$ POD modes extracted from $M = 120$ snapshots is plotted on figure 13 when the set of coefficients `KdL_mfr` has been calibrated. The first pair of modal amplitudes $a_i(t)$ for $i = 1, 2$ is well predicted on the sampling time interval ($t \in I_s$) where the trajectory is represented by the black filled circles. However, the calibration fails to predict correctly the system response on long-term time integration. After about eight periods, the response diverges. This is the result of the accumulation of errors due to the wrong approximation of the other modal amplitudes $a_i(t)$ for $i \geq 3$ which are not well reproduced, even on short-term.

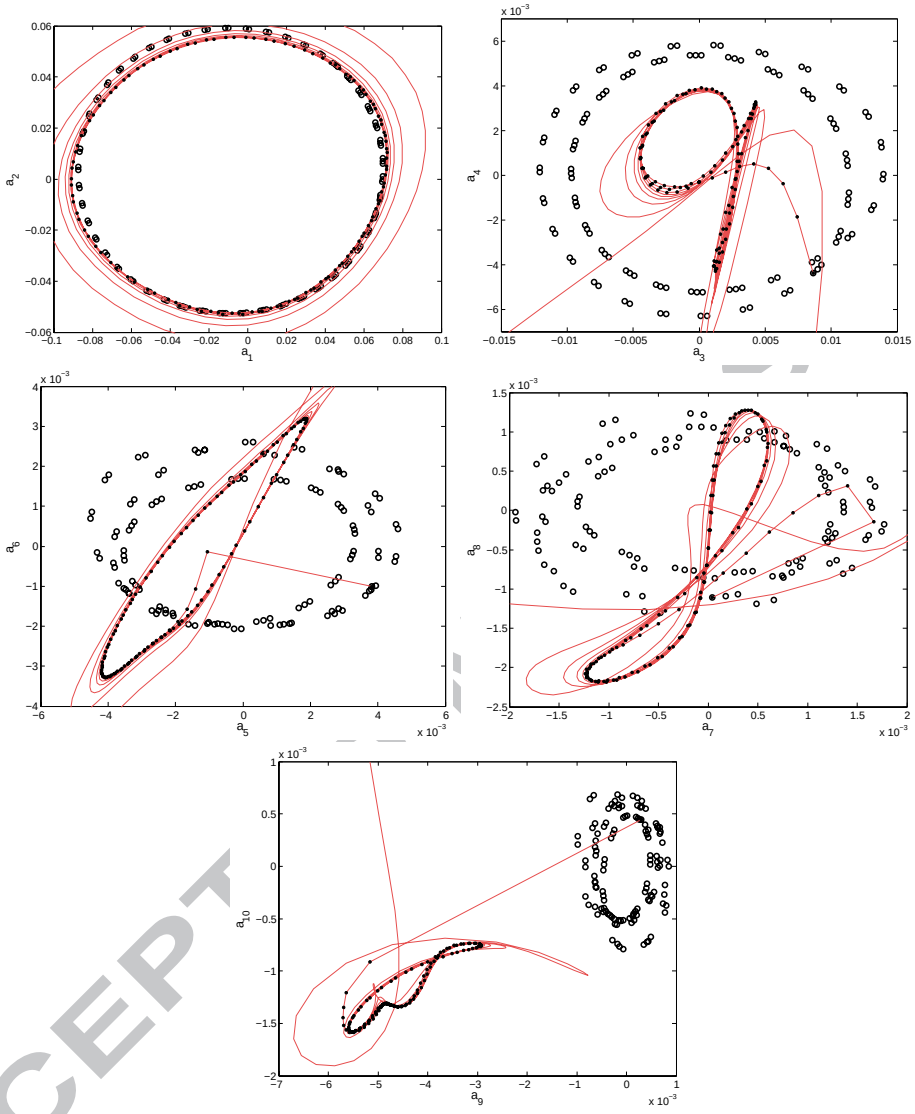

Figure 13: Comparison between the trajectories of the modal amplitudes $\{a_j(t)\}_{j=1}^{10}$ computed with the calibrated reduced-order model (—) and those of the modal amplitudes of reference $a_j^{(m)}$ obtained by the projection of the snapshots (○).

More coefficients could be considered for the calibration, but increasing the number of calibrated coefficients does not necessarily improve the accuracy on long-term. Indeed, the optimization process minimizes the error which is more important for the first leading amplitudes, but small errors on the last amplitudes are able to destabilize the response. Besides, the calibrated coefficients are sometimes far from the analytical values computed from the Galerkin projection since no regularization term has been introduced in the optimization problem (22).

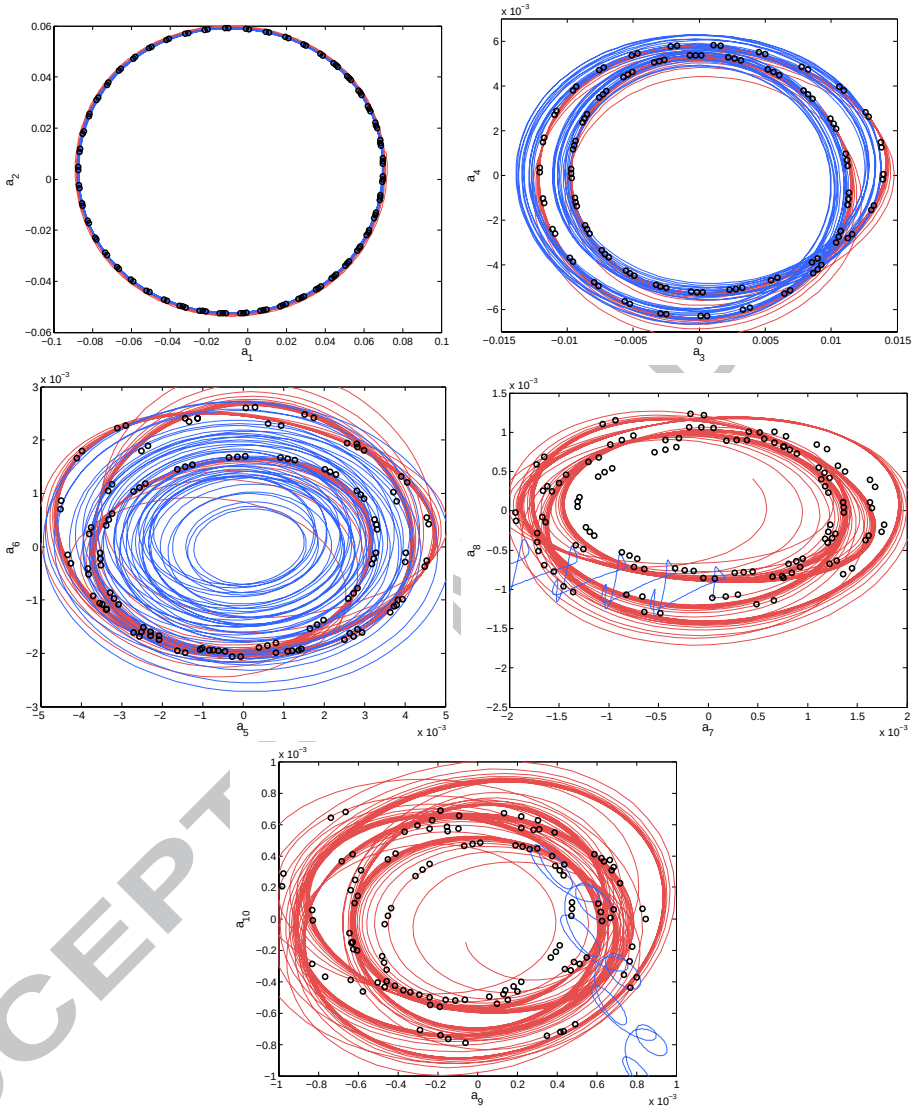

Figure 14: Comparison between the trajectories of the modal amplitudes $\{a_j(t)\}_{j=1}^{10}$ computed with the reduced-order model identified with the Tikhonov regularization (—) or with the truncated SVD method (—) and the trajectories of the modal amplitudes of reference $a_j^{(m)}$ obtained by the projection of the snapshots (○).

Identification techniques presented in section 3.2 are therefore more adapted to correct the reduced-order model since (i) the computation of optimal values is less costly and (ii) a regular-

ization term has been introduced in the least-squares problem.

A first set of coefficients for the reduced-order model is identified from the resolution of the least-squares problem (26) using the Tikhonov regularization. The regularization parameter is computed with the L-curve method and the initial guess $\mathscr{X}_0$ for the values of the coefficients is obtained by the analytical values derived in section 2.2. A second set of coefficients for the reduced-order model is computed with Eq. (27) using the truncated singular value decomposition method to approximate the pseudo-inverse. The time integration of the two reduced-order models defined by these two sets of coefficients produces now a stable response, even on long-term. The time series of the modal amplitudes are represented on figure 14. The agreement on the sampling time interval I_s is excellent and the short-term response is very accurate. The long-term behavior is also well reproduced but some discrepancies appear especially for the last modal amplitudes.

The coefficients identified as the solution of the least-squares problem regularized with the Tikhonov term produce a more reliable response for the last amplitudes. On the contrary, the coefficients identified with the truncated SVD method lead to wrong trajectories for the modal amplitudes $a_i(t)$ for $i \geq 7$. The coefficients identified for these modal amplitudes do not at all correspond to the Galerkin projection which has a physical meaning, but have rather been mathematically evaluated to match the reference response. This can be due to the truncation of the SVD which uses less than $p = 7$ singular values for some values of i. Since no initial guess for the coefficients and no regularization term are introduced in the least-squares problem (27), the coefficients can be freely identified and do not necessarily represent the physical behavior.

Macroscopic quantities like the lift coefficient which is represented on figure 15 are yet very well reproduced with both identified reduced-order models. The lift coefficient computed with the reduced-order model calibrated with `KdL_mfr` is also plotted on the first period. The agreement is rather good initially but the response diverges after about eight periods when the calibration `KdL_mfr` is used.

Finally, the errors represented on figure 16 for the modal amplitudes have been computed on the sampling time interval for the reduced-order models calibrated with `KdL_mfr`, or identified with the Tikhonov regularization or with the truncated SVD methods. The errors are significantly reduced when the coefficients are identified. It is recommended to use the identification with the Tikhonov regularization since the modal amplitudes follow the right trajectories even on long-term, and the coefficients identified are close to those computed with the analytical expressions.

6. Conclusions

In this paper, the construction of a nonlinear reduced-order model based on the proper orthogonal decomposition has been investigated for compressible flows in which a structure can move. The reduced-order model relies on the determination of an appropriate POD basis which has been computed here with an iterative method based on the QR decomposition of the truncated snapshots matrix. Comparisons with the usual snapshots method show that this method provides accurate POD modes and eigenvalues for a significantly reduced computational cost. The formulation of the Navier-Stokes equations using the modified primitive variables has been extended here to take into account the rigid body motion of a structure contained in the fluid domain. It is shown that the resulting equations are defined by an explicit set of quadratic partial differential equations which are

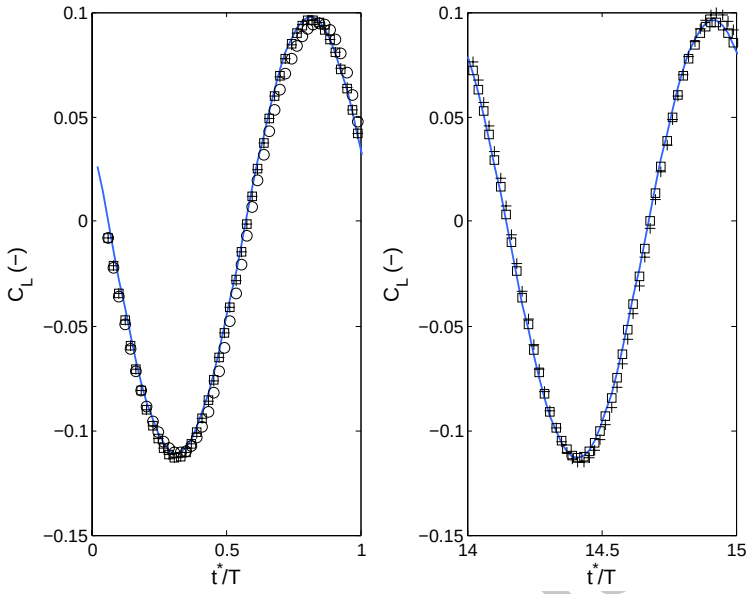

Figure 15: Comparison of the lift coefficient computed with the corrected reduced-order model: (+) least-squares identification with the Tikhonov regularization, (□) identification with the truncated SVD, (○) calibration with `KdL_mfr`. The lift is compared on the 1st and 14th period of oscillation to the reference response (—) computed with the full-order model.

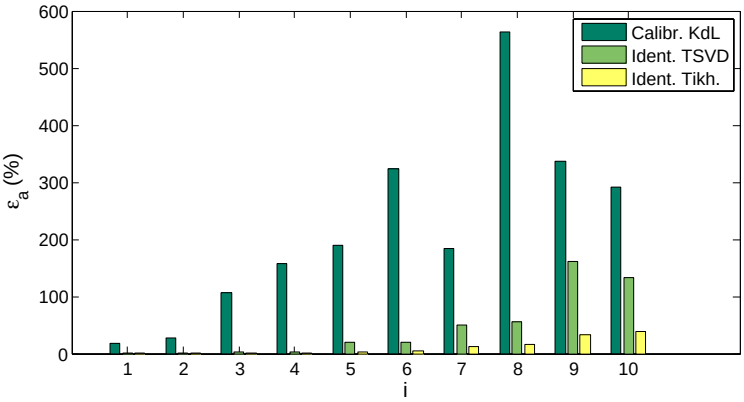

Figure 16: Comparison of the error $\overline{\varepsilon_{a_j}}$ for the modal amplitudes computed as the solution of the reduced-order model on the sampling time interval. Three different correction methods have been used here to improve the reduced-order model.

appropriate for the Galerkin projection. The reduced-order model defined by the coefficients computed from the Galerkin projection lacks however some dissipation and a correction is necessary to reproduce correctly the long-term behavior of the original full-order model. Several correction methods have been investigated in this paper. In the case of the autonomous reduced-order model, the calibration of constant and linear coefficients produces a reasonably good response compared to the reference one. However, when a non-autonomous system derived from the Euler equations is considered, the calibration is no longer sufficient. It is then recommended to turn to a more robust identification procedure using Tikhonov regularization. With such a method, the accuracy and stability of the response have indeed been significantly improved on the short- but also long-term. Future work will concern the extension to moving and deformable structures which induce not only a motion of the spatial domain but also a deformation.

Appendix A. Algorithm of the iterative subspace approximation

Algorithm Appendix A.1 presents the different steps to compute the approximation of the POD subspace by an iterative update of the QR decomposition. The update of the QR decomposition for the extended matrix $\widehat{\mathbf{Q}}_{\text{up}}$ can be performed with a classical or modified Gram-Schmidt orthogonalization process [30]. The singular vector $\mathbf{u}_{q+1}$ and the associated singular value $\widehat{\sigma}_{q+1}$ can be obtained by few steps of inverse iteration or by a singular value decomposition since the dimension of the matrix is small. The orthogonal matrix $\mathbf{G}_u$ is computed here by means of a combination of Givens rotations but a Householder transformation is advocated by [16]. The orthogonal matrix $\mathbf{G}_v$ is the result of a RQ decomposition of the product $\mathbf{G}_u^{\mathsf{T}}\widetilde{\mathbf{R}}_i$ which also produces the upper triangular matrix $\mathbf{R}_{\text{up}}$. Mastronardi et al. [48] suggest replacing the matrix $\mathbf{R}_{i-1}$ by an upper bidiagonal matrix to decrease further the computational costs of the algorithm.

At the last iteration, the matrix $\widehat{\mathbf{Q}}_M$ contains the main features of the whole snapshots database. The left and right singular subspaces – as well as the singular values – can therefore be determined by singular value decomposition of $\widehat{\mathbf{Q}}_M$. Because of the particular weighting of the snapshots, the POD subspace is obtained after several matrix operations. Indeed, $\widehat{\mathbf{Q}}_M = \widetilde{\Delta}\widetilde{\mathbf{Q}}_M\widetilde{\alpha}$ where $\widetilde{\mathbf{Q}}_M$ is the updated matrix representing the whole weighted centered snapshots database. Consequently $\widetilde{\Delta}\widetilde{\mathbf{Q}}_M\widetilde{\alpha} = \mathbf{U}\Sigma\mathbf{V}^{\mathsf{T}}$ and $\widehat{\mathbf{Q}}_M = (\widetilde{\Delta}^{-1}\mathbf{U})\,(\Sigma\mathbf{V}^{\mathsf{T}}\widetilde{\alpha}^{-1}) = \Phi\mathbf{A}$. The POD eigenvalues λ_i are finally deduced from the singular values σ_i since they are computed from a singular value decomposition [65].

References

[1] I. Akhtar, J. Borggaard, A. Hay. Shape sensitivity analysis in flow models using a finite-difference approach. *Math. Probl. Eng.* **209780** (2010), pp. 1–22.

[2] I. Akhtar, A. Nayfeh, C. Ribbens. On the stability and extension of reduced-order models in incompressible flows: A numerical study of vortex shedding. *Theor. Comput. Fuid Dyn.* **23** (3) (2009), pp. 213–237.

[3] I. Akhtar, A. H. Nayfeh. Model based control of laminar wake using fluidic actuation. *J. Comput. Nonlinear Dyn.* **5** (4) (2010), pp. 041015.

[4] J. Anttonen, P. King, P. Beran. Application of multi-POD to a pitching and plunging airfoil. *Math. Comput. Model.* **42** (3-4) (2005), pp. 245–259.

[5] N. Aubry, P. Holmes, J. Lumley, E. Stone. The dynamics of coherent structures in the wall region of a turbulent boundary layer. *J. Fluid Mech.* **192** (1988), pp. 115–173.

[6] G. Batchelor. *An introduction to fluid dynamics*, Cambridge University Press (2000).

Algorithm Appendix A.1 – Computation of the POD subspace by the iterative QR approximation.

Require: The files containing the snapshots $\boldsymbol{q}^{(m)}$ for $m = 1$ to M, the mean part $\overline{\boldsymbol{q}}$, temporal and volume weights $\widetilde{\alpha}$ and $\widetilde{\Delta}$.

{Set the submatrix $\widehat{\mathbf{Q}}_q$ as the initial approximation of the subspace}

for $i = 1$ to q **do**

Read the snapshot file and center it to get $\widetilde{\boldsymbol{q}}^{(i)} = \boldsymbol{q}^{(i)} - \overline{\boldsymbol{q}}$

Apply the temporal and volume weights and store the snapshot in the submatrix $\widehat{\mathbf{Q}}_q(:,i) = \sqrt{\alpha_i} \times \widetilde{\Delta}\, \widetilde{\boldsymbol{q}}^{(i)}$

end for

{Perform the initial QR decomposition of $\widehat{\mathbf{Q}}_q$}

$\widehat{\mathbf{Q}}_q = \mathbf{Q}_q \mathbf{R}_q$

{Update iteratively the QR decomposition}

for $i = q+1$ to M **do**

{Append a new snapshot}

Read the new snapshot $\boldsymbol{q}^{(i)}$ missing in $\widehat{\mathbf{Q}}_q$

Center it and weight it such that $\widehat{\boldsymbol{q}}^{(i)} = \sqrt{\alpha_i} \times \widetilde{\Delta}\, \widetilde{\boldsymbol{q}}^{(i)}$

{Gram-Schmidt orthogonalization of the new snapshot}

Define $\mathbf{r}_i = \mathbf{Q}_{i-1}^{\mathsf{T}} \widehat{\boldsymbol{q}}^{(i)}$ such that $\widehat{\boldsymbol{q}}^{(i)\perp} = \widehat{\boldsymbol{q}}^{(i)} - \mathbf{Q}_{i-1}\mathbf{r}_i$ is orthogonal to the columns of $\mathbf{Q}_{i-1}$. Then define $\rho_i = ||\widehat{\boldsymbol{q}}^{(i)\perp}||$ and the unit vector $\theta_i = \widehat{\boldsymbol{q}}^{(i)\perp}/\rho_i$.

{Update the QR decomposition of $\widehat{\mathbf{Q}}_{\text{up}} = [\widehat{\mathbf{Q}}_{i-1}\, \widehat{\boldsymbol{q}}^{(i)}]$}

$$\widehat{\mathbf{Q}}_{\text{up}} = \begin{bmatrix} \mathbf{Q}_{i-1}\mathbf{R}_{i-1} & \widehat{\boldsymbol{q}}^{(i)} \end{bmatrix} = \begin{bmatrix} \mathbf{Q}_{i-1} & \theta_i \end{bmatrix} \begin{bmatrix} \mathbf{R}_{i-1} & \mathbf{r}_i \\ \mathbf{0} & \rho_i \end{bmatrix} = \widetilde{\mathbf{Q}}_i \widetilde{\mathbf{R}}_i$$

Determine the smallest singular value $\widehat{\sigma}_{q+1}$ and left singular vector $\mathbf{u}_{q+1}$ of the matrix $\widetilde{\mathbf{R}}_i$.

Build the orthogonal matrix $\mathbf{G}_u$ such that $\mathbf{G}_u^{\mathsf{T}}\, \mathbf{u}_{q+1} = \mathbf{e}_{q+1} = [0 \ldots 0\, 1]^{\mathsf{T}}$

Build the orthogonal matrix $\mathbf{G}_v$ to put back $\mathbf{G}_u^{\mathsf{T}} \widetilde{\mathbf{R}}_i$ in the upper triangular form $\mathbf{R}_{\text{up}} = \mathbf{G}_u^{\mathsf{T}} \widetilde{\mathbf{R}}_i \mathbf{G}_v$

Define $\mathbf{Q}_{\text{up}} = \widetilde{\mathbf{Q}}_i \mathbf{G}_u$

Since $\widehat{\mathbf{Q}}_{\text{up}} = \widetilde{\mathbf{Q}}_i \widetilde{\mathbf{R}}_i$ by definition, the previous transformations yield $\widehat{\mathbf{Q}}_{\text{up}} = \mathbf{Q}_{\text{up}} \mathbf{R}_{\text{up}} \mathbf{G}_v^{\mathsf{T}}$.

{Update the matrices}

$\mathbf{Q}_i \leftarrow \mathbf{Q}_{\text{up}}(1 : N_v; 1 : q)$

$\mathbf{R}_i \leftarrow \mathbf{R}_{\text{up}}(1 : q; 1 : q)$

$\widehat{\mathbf{Q}}_i \leftarrow \widehat{\mathbf{Q}}_{\text{up}}(1 : N_v; 1 : q)$

end for

{Evaluate the approximate subspace and singular values}

Perform the SVD of $\widehat{\mathbf{Q}}_M = \mathbf{U}\Sigma\mathbf{V}^{\mathsf{T}}$.

Compute the POD modes $\Phi = \widetilde{\Delta}^{-1}\mathbf{U}$ and the modal amplitudes $\mathbf{A} = \Sigma\mathbf{V}^{\mathsf{T}}\widetilde{\alpha}^{-1}$. The singular values are approximated by σ_i^2 such that $\Sigma = \text{diag}(\sigma_1, \ldots, \sigma_q)$.

[7] C. Beattie, J. Borggaard, S. Gugercin, T. Iliescu. A domain decomposition approach to POD. In: Proc. 45th IEEE Conference on Decision and Control. No. FrIP14.12. (2006) pp. 6750–6756.
[8] P. Beran, D. Lucia, C. Pettit. Reduced-order modelling of limit-cycle oscillation for aeroelastic systems. *J. Fluid. Struct.* **19** (5) (2004), pp. 575–590.
[9] M. Bergmann, C.-H. Bruneau, A. Iollo. Enablers for robust POD models. *J. Comput. Phys.* **228** (2) (2009), pp. 516–538.
[10] M. Bergmann, L. Cordier, J. P. Brancher. Optimal rotary control of the cylinder wake using POD reduced-order model. *Phys. Fluid.* **17** (9) (2005), pp. 097101–20.
[11] G. Berkooz, P. Holmes, J. Lumley. The proper orthogonal decomposition in the analysis of turbulent flows. *Annu. Rev. Fluid Mech.* **25** (1993), pp. 539–575.
[12] R. Bourguet, M. Braza, A. Dervieux, A. Sévrain. Transition features in transonic flow around a NACA0012 airfoil by Navier-Stokes and low-order modelling. In: West-East High Speed Flow Field Conf., ECCOMAS. Moscow (2007).
[13] M. Buffoni, S. Camarri, A. Iollo, M. Salvetti. Low-dimensional modelling of a confined three-dimensional wake flow. *J. Fluid Mech.* **569** (2006), pp. 141–150.
[14] K. Carlberg, C. Bou-Mosleh, C. Farhat. Efficient non-linear model reduction via a least-squares Petrov-Galerkin projection and compressive tensor approximations. *Int. J. Numer. Method Eng.* **86** (2) (2011), pp.155–181.
[15] W. Cazemier, R. Verstappen, A. Veldman. Proper orthogonal decomposition and low dimensional models for driven cavity flows. *Phys. Fluid.* **10** (7) (1998), pp. 1685–1699.
[16] Y. Chahlaoui, K. Gallivan, P. Van Dooren. Recursive calculation of dominant singular subspaces. *SIAM J. Matrix Anal. Appl.* **25** (2) (2003), pp. 445–463.
[17] L. Cordier, B. Abou El Madj, J. Favier. Calibration of POD reduced-order models using Tikhonov regularization. *Int. J. Numer. Method. Fluid.* **63** (2) (2009), pp. 269–296.
[18] M. Couplet, C. Basdevant, P. Sagaut. Calibrated reduced-order POD-Galerkin system for fluid flow modelling. *J. Comput. Phys.* **207** (1) (2005), pp. 192–220.
[19] M. Couplet, P. Sagaut, C. Basdevant. Intermodal energy transfers in a proper orthogonal decomposition-Galerkin representation of a turbulent separated flows. *J. Fluid Mech.* **491** (2003), pp. 275–284.
[20] J. Donea, A. Huerta, J.-P. Ponthot, A. Rodrìguez-Ferran. *Encyclopedia of Computational Mechanics*. Vol. 1: Fundamentals, Ch. 14: Arbitrary Lagrangian-Eulerian Methods. John Wiley & Sons (2005).
[21] E. Dowell, E. Crawley, H. Curtiss, D. Peters, R. Scanlan, F. Sisto. *A modern course in aeroelasticity*, 3rd Edition, Kluwer Academic (1995).
[22] E. Dowell, K. Hall, J. Thomas, R. Florea, B. Epureanu, J. Hegg. Reduced order models in unsteady aerodynamics. In: Struct., Struct. Dyn. Mater. Conf. (1999).
[23] B. Epureanu, E. Dowell, K. Hall. Reduced-order models of unsteady transonic viscous flows in turbomachinery. *J. Fluid. Struct.* **14** (8) (2000), pp. 1215–1234.
[24] M. Fahl. Computation of POD basis functions for fluid flows with Lanczos method. *Math. Comput. Model.* **34** (1-2) (2001), pp. 91–107.
[25] R. Fletcher. *Practical methods of optimization*. Wiley (2003).
[26] B. Galletti, A. Bottaro, C. Bruneau, A. Iollo. Accurate model reduction of transient and forced wakes. *Eur. J. Mech. - B/Fluids* **26** (3) (2007), pp. 354–366.
[27] B. Galletti, C. Bruneau, L. Zannetti, A. Iollo. Low-order modelling of laminar flow regimes past a confined square cylinder. *J. Fluid Mech.* **503** (2004), pp. 161–170.
[28] M. Gazaix, A. Jolles, M. Lazareff. The elsA object-oriented computational tool for industrial applications. In: 23rd Congr. Int. Counc. Aeronaut. Sci. Toronto (2002).
[29] X. Gloerfelt. Compressible POD-Galerkin reduced-order model of self-sustained oscillations in a cavity. *AIAA J.* **1** (2006), pp. 417–444.
[30] G. Golub, C. Van Loan. *Matrix Computations*, 3rd Edition. Johns Hopkins University Press (1996).
[31] K. Hall, J. Thomas, E. Dowell. Reduced-order modelling of unsteady small-disturbance flows using a frequency-domain proper orthogonal decomposition technique. In: 37th Aerosp. Sci. Meet. Exhib. Reno (1999).
[32] P. Hansen. Truncated singular value decomposition solutions to discrete ill-posed problems with ill-determined numerical rank. *SIAM J. Sci. Statist. Comput.* **11** (3) (1990), pp. 503–518.

[33] A. Hay, I. Akhtar, J. Borggaard. On the use of sensitivity analysis in model reduction to predict flows for varying inflow conditions. *Int. J. Numer. Method. Fluid.* (2011), doi: 10.1002/fld.2512

[34] A. Hay, J. Borggaard., I. Akhtar, D. Pelletier. Reduced-order models for parameter dependent geometries based on shape sensitivity analysis. *J. Comput. Phys.* **229** (4) (2010), pp. 1327–1352.

[35] T. Henri, J.-P. Yvon. System Modeling and Optimization. Vol. 166 of IFIP International Federation for Information Processing. Springer Boston, *Ch. Convergence Estimates of POD-Galerkin Methods for Parabolic Problems*, pp. 295–306 (2005).

[36] A. Hindmarsh. ODEPACK, a systematized collection of ODE solvers. *IMACS Trans. Sci. Comput.* **1** (1983), pp. 55–64.

[37] P. Holmes, J. Lumley, G. Berkooz. *Turbulence, coherent structures, dynamical systems and symmetry*. Cambridge University Press (1996).

[38] A. Iollo. Remarks on the approximation of the Euler equations by a low order model. Research Report No. 3329, INRIA (1997).

[39] A. Iollo, S. Lanteri, J.-A. Désidéri. Stability properties of POD-Galerkin approximations for the compressible Navier-Stokes equations. *Theor. Comput. Fluid Dyn.* **13** (6) (2000), pp. 377–396.

[40] V. Kalb, A. Deane. An intrinsic stabilization scheme for proper orthogonal decomposition based low-dimensional models. *Phys. Fluid.* **19** (5) (2007), pp. 054106.

[41] M. Kirby. Minimal dynamical systems from PDEs using Sobolev eigenfunctions. *Phys. D* **57** (3-4) (1992), pp. 466–475.

[42] K. Kunisch, S. Volkwein. Galerkin proper orthogonal decomposition methods for parabolic problems. *Numer. Math.* **90** (1) (2001), pp. 117–148.

[43] E. Liberge, A. Hamdouni. Reduced order modelling method via proper orthogonal decomposition (POD) for flow around an oscillating cylinder. *J. Fluid. Struct.* **26** (2) (2010), pp. 292–311.

[44] T. Lieu, C. Farhat. Adaptation of aeroelastic reduced-order models and application to an F-16 configuration. *AIAA J.* **45** (6) (2007), pp. 1244–1257.

[45] D. Lucia, P. Beran, W. Silva. Reduced-order modeling: New approaches for computational physics. *Prog. Aerosp. Sci.* **40** (2004), pp. 51–117.

[46] D. Lucia, P. King, P. Beran. Reduced order modeling of a two-dimensional flow with moving shocks. *Comput. Fluid.* **32** (7) (2003), pp. 917–938.

[47] J. Lumley. *The structures of inhomogeneous turbulent flow*, edited by A.M. Yaglom and V.I. Tatarski, Nauka, Moscow Edition. In : Atmospheric Turbulence and Radio Wave Propagation, pp. 166–178 (1967).

[48] N. Mastronardi, M. Van Barel, R. Vandebril. A fast algorithm for the recursive calculation of dominant singular subspaces. *J. Comput. Appl. Math.* **218** (2) (2008), pp. 238–246.

[49] G.-D. Mortchéléwicz. Application of proper orthogonal decomposition to linearized Euler or Reynolds-Averaged Navier-Stokes equations. In: 47th Israel Annu. Conf. Aerosp. Sci. Tel-Aviv (2007).

[50] B. Noack, K. Afanasiev, M. Morzynski, G. Tadmor, F. Thiele. A hierarchy of low-dimensional models for the transient and post-transient cylinder wake. *J. Fluid Mech.* **497** (2003), pp. 335–363.

[51] L. Perret, E. Collin, J. Delville. Polynomial identification of POD based low-order dynamical system. *J. Turbul.* **7** (17) (2006), pp. 1–15.

[52] C. Pettit, P. Beran. Application of proper orthogonal decomposition to the discrete Euler equations. *Int. J. Numer. Method. Eng.* **55** (4) (2002), pp. 479–497.

[53] A. Placzek. Construction de modèles d'ordre réduit non-linéaires basés sur la décomposition orthogonale propre pour l'aéroélasticité. Ph.D. thesis, Conservatoire National des Arts et Métiers (2009).
URL `http://tel.archives-ouvertes.fr/tel-00461691/fr/`

[54] A. Placzek, D.-M. Tran, R. Ohayon. Hybrid proper orthogonal decomposition formulation for linear structural dynamics. *J. Sound Vib.* **318** (4-5) (2008), pp. 943–964.

[55] T. Pulliam. Low Reynolds number numerical solutions of chaotic flows. In: 27th Aerosp. Sci. Meet. No. 89-0123. Reno (1989).

[56] D. Rempfer. On low-dimensional Galerkin models for fluid flow. *Theor. Comput. Fluid Dyn.* **14** (2) (2000), pp. 75–88.

[57] C. Rowley, T. Colonius, R. Murray. Model reduction for compressible flows using POD and Galerkin projection.

Phys. D **189** (1-2) (2004), pp. 115–129.

[58] S. Siegel, K. Cohen, T. McLaughlin. Numerical simulations of a feedback controlled circular cylinder wake. *AIAA J.* **44** (6) (2006), pp. 1266–1276.

[59] S. Singh, J. Myatt, G. Addington, S. Banda, J. K. Hall. Optimal feedback control of vortex shedding using proper orthogonal decomposition models. *J. Fluid. Eng.* **123** (2001), pp. 612–618.

[60] S. Sirisup, G. Karniadakis. A spectral viscosity method for correcting the long-term behavior of POD modes. *J. Comput. Phys.* **194** (1) (2004), pp. 92–116.

[61] L. Sirovich. Turbulence and the dynamics of coherent structures, Parts I-III. *Q. Appl. Math.* **XLV** (3) (1987), pp. 561–590.

[62] S. Tang, N. Aubry. Suppression of vortex shedding inspired by a low-dimensional model. *J. Fluid. Struct.* **14** (4) (2000), pp. 443–468.

[63] J. Thomas, E. Dowell, K. Hall. Using automatic differentiation to create a nonlinear reduced-order-model aerodynamic solver. *AIAA J.* **48** (1) (2010), pp. 19–24.

[64] G. Vigo. Méthodes de décomposition orthogonale aux valeurs propres appliquées aux écoulements instationaires compressibles complexes. Ph.D. thesis, Paris IX Dauphine University (2000).

[65] S. Volkwein. Proper Orthogonal Decomposition and Singular Value Decomposition. SFB-Preprint No. 153, Graz University (1999).

[66] J. Weller, E. Lombardi, A. Iollo. Robust model identification of actuated vortex wakes. *Phys. D* **238** (4) (2009), pp. 416–427.

[67] K. Willcox. Reduced-order aerodynamic models for aeroelastic control of turbomachines. Ph.D. thesis, Massachusetts Institute of Technology (2000).

Research highlights

> A POD-Galerkin reduced-order model is developed for viscous compressible ows. > Rigid body motions are taken into account with an adequate ALE formulation. > Modi ed primitive variables are used to keep a quadratic form of the equations. > Stabilization of the reduced-order model is necessary for an accurate solution. > Identi cation with Tikhonov regularization is an e cient way of stabilization.